

# D2C: Diffusion-Decoding Models for Few-Shot Conditional Generation

**Abhishek Sinha\***

Department of Computer Science  
Stanford University  
a7b23@stanford.edu

**Jiaming Song\***

Department of Computer Science  
Stanford University  
tsong@cs.stanford.edu

**Chenlin Meng**

Department of Computer Science  
Stanford University  
chenlin@cs.stanford.edu

**Stefano Ermon**

Department of Computer Science  
Stanford University  
ermon@stanford.edu

## Abstract

Conditional generative models of high-dimensional images have many applications, but supervision signals from conditions to images can be expensive to acquire. This paper describes Diffusion-Decoding models with Contrastive representations (D2C), a paradigm for training unconditional variational autoencoders (VAEs) for few-shot conditional image generation. D2C uses a learned diffusion-based prior over the latent representations to improve generation and contrastive self-supervised learning to improve representation quality. D2C can adapt to novel generation tasks conditioned on labels or manipulation constraints, by learning from as few as 100 labeled examples. On conditional generation from new labels, D2C achieves superior performance over state-of-the-art VAEs and diffusion models. On conditional image manipulation, D2C generations are two orders of magnitude faster to produce over StyleGAN2 ones and are preferred by 50% – 60% of the human evaluators in a double-blind study.

## 1 Introduction

Generative models trained on large amounts of unlabeled data have achieved great success in various domains including images [8, 47, 72, 40], text [53, 2], audio [24, 68, 89, 59], and graphs [34, 64]. However, downstream applications of generative models are often based on various conditioning signals, such as labels [58], text descriptions [57], reward values [97], or similarity with existing data [43]. While it is possible to directly train conditional models, this often requires large amounts of paired data [54, 71] that are costly to acquire. Hence, it would be desirable to learn conditional generative models using large amounts of unlabeled data and as little paired data as possible.

Contrastive self-supervised learning (SSL) methods can greatly reduce the need for labeled data in discriminative tasks by learning effective representations from unlabeled data [91, 35, 33], and have also been shown to improve few-shot learning [37]. It is therefore natural to ask if they can also be used to improve few-shot generation. Latent variable generative models (LVGM) are a natural candidate for this, since they already involve a low-dimensional, structured latent representation of the data they generate. However, popular LVGMs, such as generative adversarial networks (GANs, [32, 47]) and diffusion models [40, 81], lack explicit tractable functions to map inputs to

---

\*Equal contribution.

representations, making it difficult to optimize latent variables with SSL. Variational autoencoders (VAEs, [49, 74]), on the other hand, can naturally adopt SSL through their encoder model, but they typically have worse sample quality.

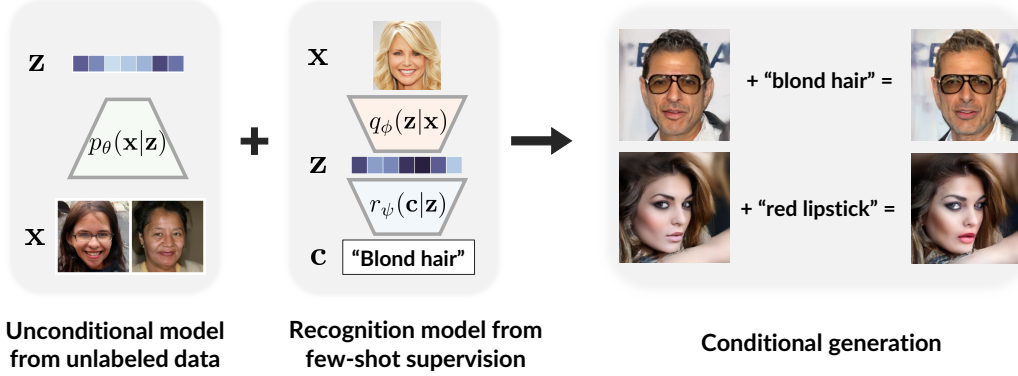


Figure 1: Few-shot conditional generation with the unconditional D2C model (left). With a recognition model over the latent space (middle), D2C can generate samples for novel conditions, such as image manipulation (right). These conditions can be defined with very few labels.

In this paper, we propose Diffusion-Decoding models with Contrastive representations (D2C), a special VAE that is suitable for conditional few-shot generation. D2C uses contrastive self-supervised learning methods to obtain a latent space that inherits the transferrability and few-shot capabilities of self-supervised representations. Unlike other VAEs, D2C learns a diffusion model over the latent representations. This latent diffusion model ensures that D2C uses the same latent distribution for both training and generation. We provide a formal argument to explain why this approach may lead to better sample quality than existing hierarchical VAEs. We further discuss how to apply D2C to few-shot conditional generation where the conditions are defined through labeled examples and/or manipulation constraints. Our approach combines a discriminative model providing conditioning signal and generative diffusion model over the latent space, and is computationally more efficient than methods that act directly over the image space (Figure 1).

We evaluate and compare D2C with several state-of-the-art generative models over 6 datasets. On unconditional generation, D2C outperforms state-of-the-art VAEs and is competitive with diffusion models under similar computational budgets. On conditional generation with 100 labeled examples, D2C significantly outperforms state-of-the-art VAE [88] and diffusion models [81]. D2C can also learn to perform certain image manipulation tasks from as few as 100 labeled examples. Notably, for manipulating images, D2C is two orders of magnitude faster than StyleGAN2 [102] and preferred by 50% – 60% of human evaluations, which to our best knowledge is the first for any VAE model.

## 2 Background

**Latent variable generative models** A latent variable generative model (LVGM) is posed as a conditional distribution  $p_\theta : \mathcal{Z} \rightarrow \mathcal{P}(\mathcal{X})$  from a latent variable  $\mathbf{z}$  to a generated sample  $\mathbf{x}$ , parametrized by  $\theta$ . To acquire new samples, LVGMs draw random latent variables  $\mathbf{z}$  from some distribution  $p(\mathbf{z})$  and map them to image samples through  $\mathbf{x} \sim p_\theta(\mathbf{x}|\mathbf{z})$ . Most LVGMs are built on top of four paradigms: variational autoencoders (VAEs, [49, 74]), Normalizing Flows (NFs, [26, 27]), Generative Adversarial Networks (GANs, [32]), and diffusion / score-based generative models [40, 82].

Particularly, VAEs use an inference model from  $\mathbf{x}$  to  $\mathbf{z}$  for training. Denoting the inference distribution from  $\mathbf{x}$  to  $\mathbf{z}$  as  $q_\phi(\mathbf{z}|\mathbf{x})$ , the generative distribution from  $\mathbf{z}$  to  $\mathbf{x}$  as  $p_\theta(\mathbf{x}|\mathbf{z})$ , VAEs are trained by minimizing the following upper bound of negative log-likelihood:

$$L_{\text{VAE}} = \mathbb{E}_{\mathbf{x} \sim p_{\text{data}}} [\mathbb{E}_{\mathbf{z} \sim q_\phi(\mathbf{z}|\mathbf{x})} [-\log p(\mathbf{x}|\mathbf{z})] + D_{\text{KL}}(q_\phi(\mathbf{z}|\mathbf{x}) \| p(\mathbf{z}))] \quad (1)$$

where  $p_{\text{data}}$  is the data distribution and  $D_{\text{KL}}$  is the KL-divergence.

**Diffusion models** Diffusion models [78, 40, 81] produce samples by reversing a Gaussian diffusion process. We use the index  $\alpha \in [0, 1]$  to denote the particular noise level of a noisy observation  $\mathbf{x}^{(\alpha)} = \sqrt{\alpha}\mathbf{x} + \sqrt{1-\alpha}\epsilon$ , where  $\mathbf{x}$  is the clean observation and  $\epsilon \sim \mathcal{N}(0, \mathbf{I})$  is a standard Gaussian distribution; as  $\alpha \rightarrow 0$ , the distribution of  $\mathbf{x}^{(\alpha)}$  converges to  $\mathcal{N}(0, \mathbf{I})$ . Diffusion models are typically parametrized as reverse noise models  $\epsilon_\theta(\mathbf{x}^{(\alpha)}, \alpha)$  that predict the noise component of  $\mathbf{x}^{(\alpha)}$  given a noise level  $\alpha$ , and trained to minimize  $\|\epsilon_\theta(\mathbf{x}^{(\alpha)}, \alpha) - \epsilon\|_2^2$ , the mean squared error loss between the true noise and predicted noise. Given any non-increasing series  $\{\alpha_i\}_{i=0}^T$  between 0 and 1, the diffusion objective for a clean sample from the data  $\mathbf{x}$  is:

$$\ell_{\text{diff}}(\mathbf{x}; w, \theta) := \sum_{i=1}^T w(\alpha_i) \mathbb{E}_{\epsilon \sim \mathcal{N}(0, \mathbf{I})} [\|\epsilon - \epsilon_\theta(\mathbf{x}^{(\alpha_i)}, \alpha_i)\|_2^2], \quad \mathbf{x}^{(\alpha_i)} := \sqrt{\alpha_i}\mathbf{x} + \sqrt{1-\alpha_i}\epsilon \quad (2)$$

where  $w : \{\alpha_i\}_{i=1}^T \rightarrow \mathbb{R}_+$  controls the loss weights for each  $\alpha$ . When  $w(\alpha) = 1$  for all  $\alpha$ , we recover the denoising score matching objective for training score-based generative models [82].

Given an initial sample  $\mathbf{x}_0 \sim \mathcal{N}(0, \mathbf{I})$ , diffusion models acquires clean samples (*i.e.*, samples of  $\mathbf{x}_1$ ) through a gradual denoising process, where samples with reducing noise levels  $\alpha$  are produced (*e.g.*,  $\mathbf{x}_0 \rightarrow \mathbf{x}_{0.3} \rightarrow \mathbf{x}_{0.7} \rightarrow \mathbf{x}_1$ ). In particular, Denoising Diffusion Implicit Models (DDIMs, [81]) uses an Euler discretization of some neural ODE [13] to produce samples (Figure 2, left).

We provide a more detailed description for training diffusion models in Appendix A.1 and sampling from DDIM in Appendix A.2. For conciseness, we use the notation  $p^{(\alpha)}(\mathbf{x}^{(\alpha)})$  to denote the marginal distribution of  $\mathbf{x}^{(\alpha)}$  under the diffusion model, and  $p^{(\alpha_1, \alpha_2)}(\mathbf{x}^{(\alpha_2)} | \mathbf{x}^{(\alpha_1)})$  to denote the diffusion sampling process from  $\mathbf{x}^{(\alpha_1)}$  to  $\mathbf{x}^{(\alpha_2)}$  (assuming  $\alpha_1 < \alpha_2$ ). This notation abstracts away the exact sampling procedure of the diffusion model, which depends on choices of  $\alpha$ .

**Self-supervised learning of representations** In self-supervised learning (SSL), representations are learned by completing certain pretext tasks that do not require extra manual labeling [65, 23]; these representations can then be applied to other downstream tasks, often in few-shot or zero-shot scenarios. In particular, contrastive representation learning encourages representations to be closer between “positive” pairs and further between “negative” pairs; contrastive predictive coding (CPC, [91]), based on multi-class classification, have been commonly used in state-of-the-art methods [35, 15, 17, 14, 79]. Other non-contrastive methods exist, such as BYOL [33] and SimSiam [16], but they usually require additional care to prevent the representation network from collapsing.

### 3 Problem Statement

**Few-shot conditional generation** Our goal is to learn an unconditional generative model  $p_\theta(\mathbf{x})$  such that it is suitable for conditional generation. Let  $\mathcal{C}(\mathbf{x}, \mathbf{c}, f)$  describe an event that “ $f(\mathbf{x}) = \mathbf{c}$ ”, where  $\mathbf{c}$  is a property value and  $f(\mathbf{x})$  is a property function that is unknown at training. In conditional generation, our goal is to sample  $\mathbf{x}$  such that the event  $\mathcal{C}(\mathbf{x}, \mathbf{c}, f)$  occurs for a chosen  $\mathbf{c}$ . If we have access to some “ground-truth” model that gives us  $p(\mathcal{C}|\mathbf{x}) := p(f(\mathbf{x}) = \mathbf{c}|\mathbf{x})$ , then the conditional model can be derived from Bayes’ rule:  $p_\theta(\mathbf{x}|\mathcal{C}) \propto p(\mathcal{C}|\mathbf{x})p_\theta(\mathbf{x})$ . These properties  $\mathbf{c}$  include (but are not limited to<sup>2</sup>) labels [58], text descriptions [57, 73], noisy or partial observations [11, 5, 44, 22], and manipulation constraints [66]. In many cases, we do not have direct access to the true  $f(\mathbf{x})$ , so we need to learn an accurate model from labeled data [6] (*e.g.*,  $(\mathbf{c}, \mathbf{x})$  pairs).

**Desiderata** Many existing methods are optimized for some known condition (*e.g.*, labels in conditional GANs [8]) or assume abundant pairs between images and conditions that can be used for pretraining (*e.g.*, DALL-E [71] and CLIP [70] over image-text pairs). Neither is the case in this paper, as we do not expect to train over paired data.

While high-quality latent representations are not essential to unconditional image generation (*e.g.*, autoregressive [90], energy-based [29], and some diffusion models [40]), they can be beneficial when we wish to specify certain conditions with limited supervision signals, similar to how SSL representations can reduce labeling efforts in downstream tasks. A compelling use case is detecting and removing biases in datasets via image manipulation, where we should not only address well-known biases a-priori but also address other hard-to-anticipate biases, adapting to societal needs [62].

<sup>2</sup>When  $\mathcal{C}$  refers to an event that is always true, we recover unconditioned generation.

Table 1: A comparison of several common paradigms for generative modeling. [Explicit  $\mathbf{x} \rightarrow \mathbf{z}$ ]: the mapping from  $\mathbf{x}$  to  $\mathbf{z}$  is directly trainable, which enables SSL; [No prior hole]: latent distributions used for generation and training are identical (Sec. 4.2), which improves generation; [Non-adversarial]: training procedure does not involve adversarial optimization, which improves training stability.

Model family	Explicit $\mathbf{x} \rightarrow \mathbf{z}$ (Enables SSL)	No prior hole (Better generation)	Non-Adversarial (Stable training)
VAE [49, 74], NF [26]	✓	✗	✓
GAN [32]	✗	✓	✗
BiGAN [28, 30]	✓	✓	✗
DDIM [81]	✗	✓	✓
<b>D2C</b>	✓	✓	✓

Therefore, a desirable generative model should not only have high sample quality but also contain informative latent representations. While VAEs are ideal for learning rich latent representations due to being able to incorporate SSL within the encoder, they generally do not achieve the same level of sample quality as GANs and diffusion models.

#### 4 Diffusion-Decoding Generative Models with Contrastive Learning

To address the above issue, we present Diffusion-Decoding generative models with Contrastive Learning (D2C), an extension to VAEs with high-quality samples and high-quality latent representations, and are thus well suited to few-shot conditional generation. Moreover, unlike GAN-based methods, D2C does not involve unstable adversarial training (Table 1).

As its name suggests, the generative model for D2C has two components – *diffusion* and *decoding*; the *diffusion* component operates over the latent space and the *decoding* component maps from latent representations to images. Let us use the  $\alpha$  index notation for diffusion random variables:  $\mathbf{z}^{(0)} \sim p^{(0)}(\mathbf{z}^{(0)}) := \mathcal{N}(0, \mathbf{I})$  is the “noisy” latent variable with  $\alpha = 0$ , and  $\mathbf{z}^{(1)}$  is the “clean” latent variable with  $\alpha = 1$ . The generative process of D2C, which we denote  $p_\theta(\mathbf{x}|\mathbf{z}^{(0)})$ , is then defined as:

$$\mathbf{z}^{(0)} \sim p^{(0)}(\mathbf{z}^{(0)}), \quad \mathbf{z}^{(1)} \sim \underbrace{p_\theta^{(0,1)}(\mathbf{z}^{(1)}|\mathbf{z}^{(0)})}_{\text{diffusion}}, \quad \mathbf{x} \sim \underbrace{p_\theta(\mathbf{x}|\mathbf{z}^{(1)})}_{\text{decoding}}, \quad (3)$$

where  $p^{(0)}(\mathbf{z}^{(0)}) = \mathcal{N}(0, \mathbf{I})$  is the prior distribution for the diffusion model,  $p_\theta^{(0,1)}(\mathbf{z}^{(1)}|\mathbf{z}^{(0)})$  is the diffusion process from  $\mathbf{z}^{(0)}$  to  $\mathbf{z}^{(1)}$ , and  $p_\theta(\mathbf{x}|\mathbf{z}^{(1)})$  is the decoder from  $\mathbf{z}^{(1)}$  to  $\mathbf{x}$ . Intuitively, D2C models produce samples by drawing  $\mathbf{z}^{(1)}$  from a diffusion process and then decoding  $\mathbf{x}$  from  $\mathbf{z}^{(1)}$ .

In order to train a D2C model, we use an inference model  $q_\phi(\mathbf{z}^{(1)}|\mathbf{x})$  that predicts proper  $\mathbf{z}^{(1)}$  latent variables from  $\mathbf{x}$ ; this can directly incorporate SSL methods [95], leading to the following objective:

$$L_{\text{D2C}}(\theta, \phi; w) := L_{\text{D2}}(\theta, \phi; w) + \lambda L_C(q_\phi), \quad (4)$$

$$L_{\text{D2}}(\theta, \phi; w) := \mathbb{E}_{\mathbf{x} \sim p_{\text{data}}, \mathbf{z}^{(1)} \sim q_\phi(\mathbf{z}^{(1)}|\mathbf{x})} [-\log p(\mathbf{x}|\mathbf{z}^{(1)}) + \ell_{\text{diff}}(\mathbf{z}^{(1)}; w, \theta)], \quad (5)$$

where  $\ell_{\text{diff}}$  is defined as in Eq.(2),  $L_C(q_\phi)$  denotes any contrastive predictive coding objective [91] with rich data augmentations [35, 15, 17, 14, 79] (details in Appendix A.3) and  $\lambda > 0$  is a weight hyperparameter. The first two terms, which we call  $L_{\text{D2}}$ , contains a “reconstruction loss” ( $-\log p(\mathbf{x}|\mathbf{z}^{(1)})$ ) and a “diffusion loss” over samples of  $\mathbf{z}^{(1)} \sim q_\phi(\mathbf{z}^{(1)}|\mathbf{x})$ . We illustrate the D2C generative and inference models in Figure 2, and its training procedure in Appendix A.4.

##### 4.1 Relationship to maximum likelihood

The D2 objective ( $L_{\text{D2}}$ ) appears similar to the original VAE objective ( $L_{\text{VAE}}$ ). Here, we make an informal statement that the D2 objective function is deeply connected to the variational lower bound of log-likelihood; we present the full statement and proof in Appendix B.1.

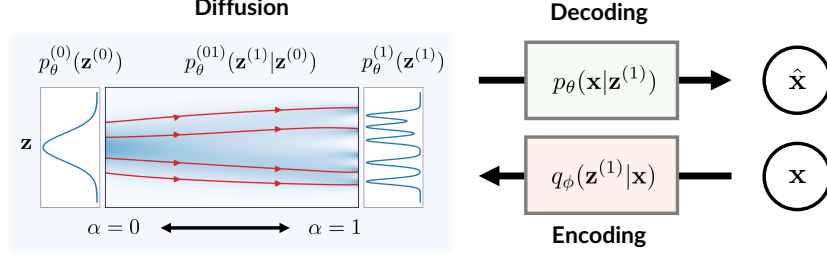


Figure 2: Illustration of components of a D2 model. On top of the encoding and decoding between  $\mathbf{x}$  and  $\mathbf{z}^{(1)}$ , we use a diffusion model to generate  $\mathbf{z}^{(1)}$  from a Gaussian  $\mathbf{z}^{(0)}$ . The red lines describe several smooth ODE trajectories from  $\alpha = 0$  to  $\alpha = 1$  corresponding to DDIM.

**Theorem 1.** (informal) For any valid  $\{\alpha_i\}_{i=0}^T$ , there exists some weights  $\hat{w} : \{\alpha_i\}_{i=1}^T \rightarrow \mathbb{R}_+$  for the diffusion objective such that  $-L_{D2}$  is a variational lower bound to the log-likelihood, i.e.,

$$-L_{D2}(\theta, \phi; \hat{w}) \leq \mathbb{E}_{p_{\text{data}}}[\log p_{\theta}(\mathbf{x})], \quad (6)$$

where  $p_{\theta}(\mathbf{x}) := \mathbb{E}_{\mathbf{z}^{(0)} \sim p^{(0)}(\mathbf{z}^{(0)})}[p_{\theta}(\mathbf{x}|\mathbf{z}^{(0)})]$  is the marginal probability of  $\mathbf{x}$  under the D2C model.

*Proof.* (sketch) The diffusion term  $\ell_{\text{diff}}$  upper bounds the KL divergence between  $q_{\phi}(\mathbf{z}_1|\mathbf{x})$  and  $p_{\theta}^{(1)}(\mathbf{z}^{(1)})$  for suitable weights [40, 81], which recovers a VAE objective.  $\square$

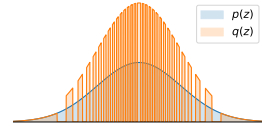
## 4.2 D2C models address latent posterior mismatch in VAEs

While D2C is a special case of VAE, we argue that D2C is non-trivial in the sense that it addresses a long-standing problem in VAE methods [87, 84], namely the mismatch between the prior distribution  $p_{\theta}(\mathbf{z})$  and the aggregate (approximate) posterior distribution  $q_{\phi}(\mathbf{z}) := \mathbb{E}_{p_{\text{data}}(\mathbf{x})}[q_{\phi}(\mathbf{z}|\mathbf{x})]$ . A mismatch could create “holes” [76, 41, 3] in the prior that the aggregate posterior fails to cover during training, resulting in worse sample quality, as many latent variables used during generation are likely to never have been trained on. We formalize this notion in the following definition.

**Definition 1** (Prior hole). Let  $p(\mathbf{z}), q(\mathbf{z})$  be two distributions with  $\text{supp}(q) \subseteq \text{supp}(p)$ . We say that  $q$  has an  $(\epsilon, \delta)$ -prior hole with respect to (the prior)  $p$  for  $\epsilon, \delta \in (0, 1)$ ,  $\delta > \epsilon$ , if there exists a set  $S \in \text{supp}(P)$ , such that  $\int_S p(\mathbf{z})d\mathbf{z} \geq \delta$  and  $\int_S q(\mathbf{z})d\mathbf{z} \leq \epsilon$ .

Intuitively, if  $q_{\phi}(\mathbf{z})$  has a prior hole with large  $\delta$  and small  $\epsilon$  (e.g., inversely proportional to the number of training samples), then it is very likely that latent variables within the hole are never seen during training (small  $\epsilon$ ), yet frequently used to produce samples (large  $\delta$ ). Most existing methods address this problem by optimizing certain statistical divergences between  $q_{\phi}(\mathbf{z})$  and  $p_{\theta}(\mathbf{z})$ , such as the KL divergence or Wasserstein distance [85]. However, we argue in the following statement that prior holes might not be eliminated even if we optimize certain divergence values to be reasonably low, especially when  $q_{\phi}(\mathbf{z})$  is very flexible. We present the formal statement and proof in Appendix B.2.

**Theorem 2.** (informal) Let  $p_{\theta}(\mathbf{z}) = \mathcal{N}(0, 1)$ . For any  $\epsilon > 0$ , there exists a distribution  $q_{\phi}(\mathbf{z})$  with an  $(\epsilon, 0.49)$ -prior hole, such that  $D_{\text{KL}}(q_{\phi}||p_{\theta}) \leq \log 2^3$  and  $W_2(q_{\phi}, p_{\theta}) < \gamma$  for any  $\gamma > 0$ , where  $W_2$  is the 2-Wasserstein distance.



*Proof.* (sketch) We construct a  $q_{\phi}$  that satisfies these properties (top-right figure). First, we truncate the Gaussian and divide them into regions with same probability mass; then we support  $q_{\phi}$  over half of these regions (so  $\delta > 0.49$ ); finally, we show that the divergences are small enough.  $\square$

In contrast to addressing prior holes by optimization, diffusion models eliminate prior holes by construction, since the diffusion process from  $\mathbf{z}^{(1)}$  to  $\mathbf{z}^{(0)}$  is constructed such that the distribution of  $\mathbf{z}^{(\alpha)}$  always converges to a standard Gaussian as  $\alpha \rightarrow 0$ . As a result, the distribution of latent

<sup>3</sup>This is reasonably low for realistic VAE models (NVAE [88] reports a KL divergence of around 2810 nats).

variables used during training is arbitrarily close to that used in generation<sup>4</sup>, which is also the case in GANs. Therefore, our argument provides an explanation as to why we observe better sample quality results from GANs and diffusion models than VAEs and NFs.

## 5 Few-shot Conditional Generation with D2C

In this section, we discuss how D2C can be used to learn to perform conditional generation from few-shot supervision. We note that D2C is only trained on images and not with any other data modalities (*e.g.*, image-text pairs [71]) or supervision techniques (*e.g.*, meta-learning [20, 6]).

**Algorithm** We describe the general algorithm for conditional generation from a few images in Algorithm 1, and detailed implementations in Appendix C. With a model over the latent space (denoted as  $r_\psi(\mathbf{c}|\mathbf{z}^{(1)})$ ), we draw conditional latents from an unnormalized distribution with the diffusion prior (line 4). This can be implemented in many ways such as rejection sampling or Langevin dynamics [63, 83, 25].

---

### Algorithm 1 Conditional generation with D2C

---

- 1: **Input**  $n$  examples  $\{(\mathbf{x}_i, \mathbf{c}_i)\}_{i=1}^n$ , property  $\mathbf{c}$ .
  - 2: Acquire latents  $\mathbf{z}_i^{(1)} \sim q_\phi(\mathbf{z}^{(1)}|\mathbf{x}_i)$  for  $i \in [n]$ ;
  - 3: Train model  $r_\psi(\mathbf{c}|\mathbf{z}^{(1)})$  over  $\{(\mathbf{z}_i^{(1)}, \mathbf{c}_i)\}_{i=1}^n$
  - 4: Sample latents with  $\hat{\mathbf{z}}^{(1)} \sim r_\psi(\mathbf{c}|\mathbf{z}^{(1)}) \cdot p_\theta^{(1)}(\mathbf{z}^{(1)})$  (unnormalized);
  - 5: Decode  $\hat{\mathbf{x}} \sim p_\theta(\mathbf{x}|\hat{\mathbf{z}}^{(1)})$ .
  - 6: **Output**  $\hat{\mathbf{x}}$ .
- 

**Conditions from labeled examples** Given a few labeled examples, we wish to produce diverse samples with a certain label. For labeled examples we can directly train a classifier over the latent space, which we denote as  $r_\psi(\mathbf{c}|\mathbf{z}^{(1)})$  with  $\mathbf{c}$  being the class label and  $\mathbf{z}^{(1)}$  being the latent representation of  $\mathbf{x}$  from  $q_\phi(\mathbf{z}^{(1)}|\mathbf{x})$ . If these examples do not have labels (*i.e.*, we merely want to generate new samples similar to given ones), we can train a positive-unlabeled (PU) classifier [31] where we assign “positive” to the new examples and “unlabeled” to training data. Then we use the classifier with the diffusion model  $p_\theta(\mathbf{z}^{(1)}|\mathbf{z}^{(0)})$  to produce suitable values of  $\mathbf{z}^{(1)}$ , such as by rejecting samples from the diffusion model that has a small  $r_\psi(\mathbf{c}|\mathbf{z}^{(1)})$ .

**Conditions from manipulation constraints** Given a few labeled examples, here we wish to learn how to manipulate images. Specifically, we condition over the event that “ $\mathbf{x}$  has label  $\mathbf{c}$  but is similar to image  $\bar{\mathbf{x}}$ ”. Here  $r_\psi(\mathbf{c}|\mathbf{z}^{(1)})$  is the unnormalized product between the classifier conditional probability and closeness to the latent  $\bar{\mathbf{z}}^{(1)}$  of  $\bar{\mathbf{x}}$  (*e.g.*, measured with RBF kernel). We implement line 4 of Alg. 1 with a Lanvegin-like procedure where we take a gradient step with respect to the classifier probability and then correct this gradient step with the diffusion model. Unlike many GAN-based methods [12, 69, 93, 43, 94], D2C does not need to optimize an inversion procedure at evaluation time, and thus the latent value is much faster to compute; D2C is also better at retaining fine-grained features of the original image due to the reconstruction loss.

## 6 Related Work

**Latent variable generative models** Most deep generative models explicitly define a latent representation, except for some energy-based models [39, 29] and autoregressive models [90, 89, 10]. Unlike VAEs and NFs, GANs do not explicitly define an inference model and instead optimize a two-player game. In terms of sample quality, GANs currently achieve superior performance over VAEs and NFs, but they can be difficult to invert even with additional optimization [45, 96, 7]. This can be partially addressed by training reconstruction-based losses with GANs [51, 52]. Moreover, the GAN training procedure can be unstable [9, 8, 60], lack a informative objective for measuring progress [4], and struggle with discrete data [98]. Diffusion models [25] achieves high sample quality without adversarial training, but its latent dimension must be equal to the image dimension.

**Addressing posterior mismatch in VAEs** Most methods address this mismatch problem by improving inference models [61, 48, 86], prior models [87, 3, 84], or objective functions [99, 100, 101, 1, 56]; all these approaches optimize the posterior model to be close to the prior. In Section 4.2, we explain why these approaches do not necessarily remove large “prior holes”, so their sample

---

<sup>4</sup>We expand this argument in Appendix B.2.



qualities remain relatively poor even after many layers [88, 18]. Other methods adopt a “two-stage” approach [21], which fits a generative model over the latent space of autoencoders [92, 72, 24, 71].

**Conditional generation with unconditional models** To perform conditional generation over an unconditional LVGM, most methods assume access to a discriminative model (*e.g.*, a classifier); the latent space of the generator is then modified to change the outputs of the discriminative model. The discriminative model can operate on either the image space [63, 67, 25] or the latent space [77, 94]. For image space discriminative models, plug-and-play generative networks [63] control the attributes of generated images via Langevin dynamics [75]; these ideas are also explored in diffusion models [83]. Image manipulation methods are based on GANs often operate with latent space discriminators [77, 94]. However, these methods have some trouble manipulating real images because of imperfect reconstruction [103, 7]. This is not a problem in D2C since a reconstruction objective is optimized.

## 7 Experiments

We examine the conditional and unconditional generation qualities of D2C over CIFAR-10 [50], CIFAR-100 [50], fMoW [19], CelebA-64 [55], CelebA-HQ-256 [45], and FFHQ-256 [46]. Our D2C implementation is based on the state-of-the-art NVAE [88] autoencoder structure, the U-Net diffusion model [40], and the MoCo-v2 contrastive representation learning method [15]. We keep the diffusion series hyperparameter  $\{\alpha_i\}_{i=1}^T$  identical to ensure a fair comparison with different diffusion models. For the contrastive weight hyperparameter  $\lambda$  in Equation (4), we consider the value of  $\lambda = 10^{-4}$  based on the relative scale between the  $L_C$  and  $L_{D2}$ ; we find that the results are relatively insensitive to  $\lambda$ . We use 100 diffusion steps for DDIM and D2C unless mentioned otherwise, as running with longer steps is not computationally economical despite tiny gains in FID [81]. We include additional training details, such as architectures, optimizers and learning rates in Appendix C.

Table 2: Quality of representations and generations with LVGMs.

Model	CIFAR-10			CIFAR-100			fMoW		
	FID ↓	MSE ↓	Acc ↑	FID ↓	MSE ↓	Acc ↑	FID ↓	MSE ↓	Acc ↑
NVAE [88]	36.4	<b>0.25</b>	18.8	42.5	0.53	4.1	82.25	<b>0.30</b>	27.7
DDIM [81]	<b>4.16</b>	2.5	22.5	<b>10.16</b>	3.2	2.2	<b>37.74</b>	3.0	23.5
D2C (Ours)	10.15	0.76	<b>76.02</b>	14.62	<b>0.44</b>	<b>42.75</b>	44.7	2.33	<b>66.9</b>

### 7.1 Unconditional generation

For unconditional generation, we measure the sample quality of images using the Frechet Inception Distance (FID, [38]) with 50,000 images. In particular, we extensively evaluate NVAE [88] and DDIM [81], a competitive VAE model and a competitive diffusion model as baselines because we can directly obtain features from them without additional optimization steps<sup>5</sup>. For them, we report mean-squared reconstruction error (MSE, summed over all pixels, pixels normalized to  $[0, 1]$ ) and linear classification accuracy (Acc., measured in percentage) over  $\mathbf{z}_1$  features for the test set.

We report sample quality results<sup>6</sup> in Tables 2, and 3. For FID, we outperform NVAE in all datasets and outperform DDIM on CelebA-64 and CelebA-HQ-256, which suggests our results are competitive with state-of-the-art non-adversarial generative models. In Table 2, we additionally compare NVAE, DDIM and D2C in terms of reconstruction and linear classification accuracy. As all three methods contain reconstruction losses, the MSE values are low and comparable. However, D2C enjoys much better linear classification accuracy than the other two thanks to the contrastive SSL component. We further note that training the same contrastive SSL method without  $L_{D2}$  achieves slightly higher 78.3% accuracy on CIFAR-10. We tried improving this via ResNet [36] encoders, but this significantly increased reconstruction error, possibly due to loss of information in average pooling layers.

<sup>5</sup>For DDIM, the latent representations  $\mathbf{x}^{(0)}$  are obtained by reversing the neural ODE process.

<sup>6</sup>Due to space limits, we place additional CIFAR-10 results in Appendix D.



Figure 3: Generated samples on CIFAR-10 (left), fMoW (mid), and FFHQ  $256 \times 256$  (right).

Table 3: FID scores over different faces dataset with LVGMs.

Model	CelebA-64	CelebA-HQ-256	FFHQ-256
NVAE [88]	13.48	40.26	26.02
DDIM [81]	6.53	25.6	-
D2C (Ours)	<b>5.7</b>	<b>18.74</b>	<b>13.04</b>

Table 4: Sample quality as a function of diffusion steps.

Steps	CIFAR-10			CIFAR-100			CelebA-64		
	10	50	100	10	50	100	10	50	100
DDPM [40]	41.07	8.01	5.78	50.27	21.37	16.72	33.12	18.48	13.93
DDIM [81]	<b>13.36</b>	<b>4.67</b>	<b>4.16</b>	<b>23.34</b>	<b>11.69</b>	<b>10.16</b>	17.33	9.17	6.53
D2C (Ours)	17.71	10.11	10.15	23.16	14.62	14.46	<b>17.32</b>	<b>6.8</b>	<b>5.7</b>

## 7.2 Few-shot conditional generation from examples

We demonstrate the advantage of D2C representations by performing few-shot conditional generation over labels. We consider two types of labeled examples: one has binary labels for which we train a binary classifier; the other is positive-only labeled (*e.g.*, images of female class) for which we train a PU classifier. Our goal here is to generate a diverse group of images with a certain label. We evaluate and compare three models: D2C, NVAE and DDIM. We train a classifier  $r_\psi(c|z)$  over the latent space of these models; we also train a image space classifier and use it with DDIM (denoted as DDIM-I). We run Algorithm 1 for these models, where line 4 is implemented via rejection sampling. As our goal is to compare different models, we leave more sophisticated methods [25] as future work.

We consider performing 8 conditional generation tasks over CelebA-64 with 2 binary classifiers (trained over 100 samples, 50 for each class) and 4 PU classifiers (trained over 100 positively labeled and 10k unlabeled samples). We also report a “naive” approach where we use all the training images (regardless of labels) and compute its FID with the corresponding subset of images (*e.g.*, all images versus blond images). In Table 5, we report the FID score between generated images (5k samples) and real images of the corresponding label. These results suggest that D2C outperforms the other approaches, and is the only one that performs better than the “naive” approach in most cases, illustrating the advantage of contrastive representations for few-shot conditional generation.

## 7.3 Few-shot conditional generation from manipulation constraints

Finally, we consider image manipulation where we use binary classifiers that are learned over 50 labeled instances for each class. We perform Amazon Mechanical Turk (AMT) evaluations over two attributes in the CelebA-256 dataset, *blond* and *red lipstick*, over D2C, DDIM, NVAE and StyleGAN2 [47] (see Figure 4). The evaluation is double-blinded: neither we nor the evaluators know the correspondence between generated image and underlying model during the study. We include



Table 5: FID scores for few-shot conditional generation with various types of labeled examples. Naive performs very well for non-blond due to class percentages.

Method	Classes (% in train set)	D2C	DDIM	NVAE	DDIM-I	Naive
Binary	Male (42%)	<b>13.44</b>	38.38	41.07	29.03	26.34
	Female (58%)	<b>9.51</b>	19.25	16.57	15.17	18.72
	Blond (15%)	<b>17.61</b>	31.39	31.24	29.09	27.51
	Non-Blond (85%)	<b>8.94</b>	9.67	16.73	19.76	3.77
PU	Male (42%)	<b>16.39</b>	37.03	42.78	19.60	26.34
	Female (58%)	<b>12.21</b>	15.42	18.36	14.96	18.72
	Blond (15%)	<b>10.09</b>	30.20	31.06	76.52	27.51
	Non-Blond (85%)	<b>9.09</b>	9.70	17.98	9.90	3.77

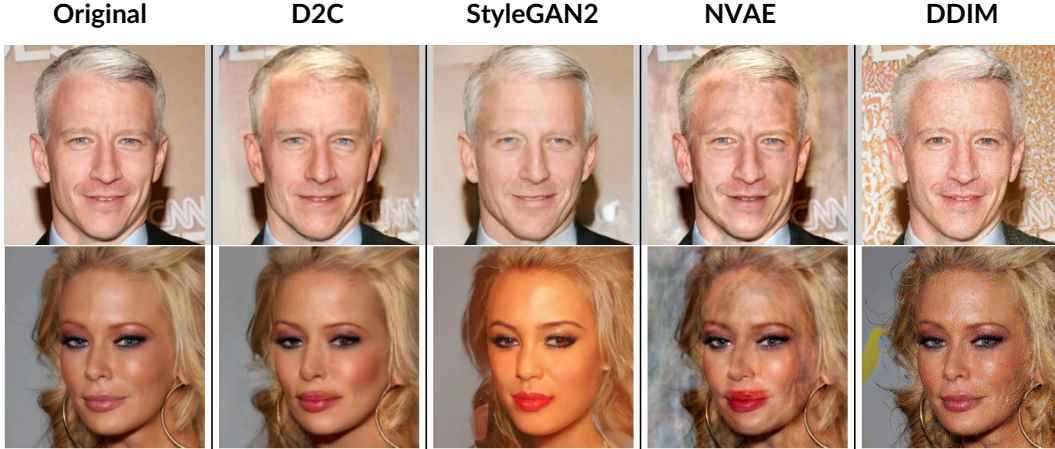


Figure 4: Image manipulation results for *blond* (top) and *red lipstick* (bottom). D2C is better than StyleGAN2 at preserving details of the original image, such as eyes, earrings, and background.

more details (algorithm, setup and human evaluation) in Appendix C and additional qualitative results (such as *beard* and *gender* attributes) in Appendix D.

In Figure 7, we show the percentage of manipulations preferred by AMT evaluators for each model; D2C slightly outperforms StyleGAN2 for *blond* and significantly outperforms StyleGAN2 for *red lipstick*. When we compare D2C with only StyleGAN2, D2C is preferred over 51.5% for *blond* and 60.8% for *red lipstick*. An additional advantage of D2C is that the manipulation is much faster than StyleGAN2, since the latter requires additional optimization over the latent space to improve reconstruction [102]. On the same Nvidia 1080Ti GPU, it takes 0.013 seconds to obtain the latent code in D2C, while the same takes 8 seconds [102] for StyleGAN2 (615 $\times$  slower). As decoding is very fast for both models, D2C generations are around two orders of magnitude faster to produce.

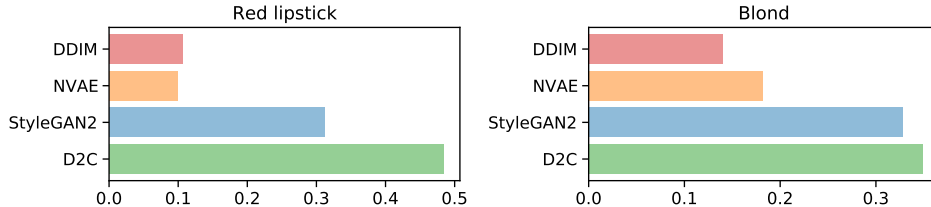


Figure 5: AMT evaluation over image manipulations.  $x$ -axis shows the percentage that the evaluator selects the image generated from the corresponding model out of 4 images from each model.

## 8 Discussions and Limitations

We introduced D2C, a VAE-based generative model with a latent space suitable for few-shot conditional generation. To our best knowledge, our model is the first unconditional VAE to demonstrate superior image manipulation performance than StyleGAN2, which is surprising given our use of a regular NVAE architecture. We believe that with better architectures, such as designs from StyleGAN2 or Transformers [42], D2C can achieve even better performance. It is also interesting to formally investigate the integration between D2C and other types of conditions on the latent space, as well as training D2C in conjunction with other domains and data modalities, such as text [71], in a fashion that is similar to semi-supervised learning. Nevertheless, we note that our model have to be used properly in order to mitigate potential negative societal impacts, such as deep fakes.

## Acknowledgements

This research was supported by NSF (#1651565, #1522054, #1733686), ONR (N00014-19-1-2145), AFOSR (FA9550-19-1-0024), Amazon AWS, Stanford Institute for Human-Centered Artificial Intelligence (HAI), and Google Cloud.

## References

- [1] Alexander A Alemi, Ben Poole, Ian Fischer, Joshua V Dillon, Rif A Saurous, and Kevin Murphy. Fixing a broken ELBO. *arXiv preprint arXiv:1711.00464*, November 2017.
- [2] Jyoti Aneja, Harsh Agrawal, Dhruv Batra, and Alexander Schwing. Sequential latent spaces for modeling the intention during diverse image captioning. In *Proceedings of the IEEE/CVF International Conference on Computer Vision*, pages 4261–4270, 2019.
- [3] Jyoti Aneja, Alexander Schwing, Jan Kautz, and Arash Vahdat. NCP-VAE: Variational autoencoders with noise contrastive priors. *arXiv preprint arXiv:2010.02917*, October 2020.
- [4] Martin Arjovsky, Soumith Chintala, and Léon Bottou. Wasserstein GAN. *arXiv preprint arXiv:1701.07875*, January 2017.
- [5] Muhammad Asim, Ali Ahmed, and Paul Hand. Invertible generative models for inverse problems: mitigating representation error and dataset bias. *arXiv preprint arXiv:1905.11672*, May 2019.
- [6] Sergey Bartunov and Dmitry Vetrov. Few-shot generative modelling with generative matching networks. In Amos Storkey and Fernando Perez-Cruz, editors, *Proceedings of the Twenty-First International Conference on Artificial Intelligence and Statistics*, volume 84 of *Proceedings of Machine Learning Research*, pages 670–678. PMLR, 2018.
- [7] David Bau, Jun-Yan Zhu, Jonas Wulff, William Peebles, Hendrik Strobelt, Bolei Zhou, and Antonio Torralba. Seeing what a gan cannot generate. In *Proceedings of the IEEE/CVF International Conference on Computer Vision*, pages 4502–4511, 2019.
- [8] Andrew Brock, Jeff Donahue, and Karen Simonyan. Large scale GAN training for high fidelity natural image synthesis. *arXiv preprint arXiv:1809.11096*, September 2018.
- [9] Andrew Brock, Theodore Lim, James M Ritchie, and Nick Weston. Neural photo editing with introspective adversarial networks. *arXiv preprint arXiv:1609.07093*, 2016.
- [10] Tom B Brown, Benjamin Mann, Nick Ryder, Melanie Subbiah, Jared Kaplan, Prafulla Dhariwal, Arvind Neelakantan, Pranav Shyam, Girish Sastry, Amanda Askell, Sandhini Agarwal, Ariel Herbert-Voss, Gretchen Krueger, Tom Henighan, Rewon Child, Aditya Ramesh, Daniel M Ziegler, Jeffrey Wu, Clemens Winter, Christopher Hesse, Mark Chen, Eric Sigler, Mateusz Litwin, Scott Gray, Benjamin Chess, Jack Clark, Christopher Berner, Sam McCandlish, Alec Radford, Ilya Sutskever, and Dario Amodei. Language models are Few-Shot learners. *arXiv preprint arXiv:2005.14165*, May 2020.
- [11] Emmanuel J Candes, Justin K Romberg, and Terence Tao. Stable signal recovery from incomplete and inaccurate measurements. *Communications on Pure and Applied Mathematics: A Journal Issued by the Courant Institute of Mathematical Sciences*, 59(8):1207–1223, 2006.
- [12] Qifeng Chen and Vladlen Koltun. Photographic image synthesis with cascaded refinement networks. In *ICCV*, 2017.

- [13] Ricky T Q Chen, Yulia Rubanova, Jesse Bettencourt, and David Duvenaud. Neural ordinary differential equations. *arXiv preprint arXiv:1806.07366*, June 2018.
- [14] Ting Chen, Simon Kornblith, Mohammad Norouzi, and Geoffrey Hinton. A simple framework for contrastive learning of visual representations. *arXiv preprint arXiv:2002.05709*, February 2020.
- [15] Xinlei Chen, Haoqi Fan, Ross Girshick, and Kaiming He. Improved baselines with momentum contrastive learning. *arXiv preprint arXiv:2003.04297*, March 2020.
- [16] Xinlei Chen and Kaiming He. Exploring simple siamese representation learning. *arXiv preprint arXiv:2011.10566*, November 2020.
- [17] Xinlei Chen, Saining Xie, and Kaiming He. An empirical study of training Self-Supervised vision transformers. *arXiv preprint arXiv:2104.02057*, April 2021.
- [18] Rewon Child. Very deep vaes generalize autoregressive models and can outperform them on images. *arXiv preprint arXiv:2011.10650*, 2020.
- [19] Gordon Christie, Neil Fendley, James Wilson, and Ryan Mukherjee. Functional map of the world. In *Proceedings of the IEEE Conference on Computer Vision and Pattern Recognition*, pages 6172–6180, 2018.
- [20] Louis Clouâtre and Marc Demers. Figr: Few-shot image generation with reptile. *arXiv preprint arXiv:1901.02199*, 2019.
- [21] Bin Dai and David Wipf. Diagnosing and enhancing VAE models. *arXiv preprint arXiv:1903.05789*, March 2019.
- [22] Giannis Daras, Joseph Dean, Ajil Jalal, and Alexandros G Dimakis. Intermediate layer optimization for inverse problems using deep generative models. *arXiv preprint arXiv:2102.07364*, February 2021.
- [23] Jacob Devlin, Ming-Wei Chang, Kenton Lee, and Kristina Toutanova. BERT: Pre-training of deep bidirectional transformers for language understanding. *arXiv preprint arXiv:1810.04805*, October 2018.
- [24] Prafulla Dhariwal, Heewoo Jun, Christine Payne, Jong Wook Kim, Alec Radford, and Ilya Sutskever. Jukebox: A generative model for music. *arXiv preprint arXiv:2005.00341*, 2020.
- [25] Prafulla Dhariwal and Alex Nichol. Diffusion models beat GANs on image synthesis. *arXiv preprint arXiv:2105.05233*, May 2021.
- [26] L Dinh, D Krueger, and Y Bengio. NICE: Non-linear independent components estimation. *arXiv preprint arXiv:1410.8516*, 2014.
- [27] Laurent Dinh, Jascha Sohl-Dickstein, and Samy Bengio. Density estimation using real NVP. *arXiv preprint arXiv:1605.08803*, May 2016.
- [28] Jeff Donahue, Philipp Krähenbühl, and Trevor Darrell. Adversarial feature learning. *arXiv preprint arXiv:1605.09782*, May 2016.
- [29] Yilun Du and Igor Mordatch. Implicit generation and generalization in Energy-Based models. *arXiv preprint arXiv:1903.08689*, March 2019.
- [30] Vincent Dumoulin, Ishmael Belghazi, Ben Poole, Olivier Mastropietro, Alex Lamb, Martin Arjovsky, and Aaron Courville. Adversarially learned inference. *arXiv preprint arXiv:1606.00704*, June 2016.
- [31] Charles Elkan and Keith Noto. Learning classifiers from only positive and unlabeled data. In *14th ACM SIGKDD*, pages 213–220, 2008.
- [32] Ian Goodfellow, Jean Pouget-Abadie, Mehdi Mirza, Bing Xu, David Warde-Farley, Sherjil Ozair, Aaron Courville, and Yoshua Bengio. Generative adversarial nets. In Z Ghahramani, M Welling, C Cortes, N D Lawrence, and K Q Weinberger, editors, *Advances in Neural Information Processing Systems 27*, pages 2672–2680. Curran Associates, Inc., 2014.
- [33] Jean-Bastien Grill, Florian Strub, Florent Altché, Corentin Tallec, Pierre H Richemond, Elena Buchatskaya, Carl Doersch, Bernardo Avila Pires, Zhaohan Daniel Guo, Mohammad Gheshlaghi Azar, Bilal Piot, Koray Kavukcuoglu, Rémi Munos, and Michal Valko. Bootstrap your own latent: A new approach to Self-Supervised learning. *arXiv preprint arXiv:2006.07733*, June 2020.

- [34] Aditya Grover, Aaron Zweig, and Stefano Ermon. Graphite: Iterative generative modeling of graphs. In *International conference on machine learning*, pages 2434–2444. PMLR, 2019.
- [35] Kaiming He, Haoqi Fan, Yuxin Wu, Saining Xie, and Ross Girshick. Momentum contrast for unsupervised visual representation learning. *arXiv preprint arXiv:1911.05722*, November 2019.
- [36] Kaiming He, Xiangyu Zhang, Shaoqing Ren, and Jian Sun. Deep residual learning for image recognition. *arXiv preprint arXiv:1512.03385*, December 2015.
- [37] Olivier Henaff. Data-efficient image recognition with contrastive predictive coding. In *International Conference on Machine Learning*, pages 4182–4192. PMLR, 2020.
- [38] Martin Heusel, Hubert Ramsauer, Thomas Unterthiner, Bernhard Nessler, and Sepp Hochreiter. GANs trained by a two Time-Scale update rule converge to a local nash equilibrium. *arXiv preprint arXiv:1706.08500*, June 2017.
- [39] Geoffrey E Hinton. Training products of experts by minimizing contrastive divergence. *Neural computation*, 14(8):1771–1800, August 2002.
- [40] Jonathan Ho, Ajay Jain, and Pieter Abbeel. Denoising diffusion probabilistic models. *arXiv preprint arXiv:2006.11239*, June 2020.
- [41] Matthew D Hoffman and Matthew J Johnson. Elbo surgery: yet another way to carve up the variational evidence lower bound. In *Workshop in Advances in Approximate Bayesian Inference, NIPS*, volume 1, page 2. approximateinference.org, 2016.
- [42] Drew A Hudson and C Lawrence Zitnick. Generative adversarial transformers. *arXiv preprint arXiv:2103.01209*, 2021.
- [43] Phillip Isola, Jun-Yan Zhu, Tinghui Zhou, and Alexei A Efros. Image-to-image translation with conditional adversarial networks. In *CVPR*, 2017.
- [44] Zahra Kadkhodaie and Eero P Simoncelli. Solving linear inverse problems using the prior implicit in a denoiser. *arXiv preprint arXiv:2007.13640*, July 2020.
- [45] Tero Karras, Timo Aila, Samuli Laine, and Jaakko Lehtinen. Progressive growing of GANs for improved quality, stability, and variation. *arXiv preprint arXiv:1710.10196*, October 2017.
- [46] Tero Karras, Samuli Laine, and Timo Aila. A Style-Based generator architecture for generative adversarial networks. *arXiv preprint arXiv:1812.04948*, December 2018.
- [47] Tero Karras, Samuli Laine, Miika Aittala, Janne Hellsten, Jaakko Lehtinen, and Timo Aila. Analyzing and improving the image quality of stylegan. In *Proceedings of the IEEE/CVF Conference on Computer Vision and Pattern Recognition*, pages 8110–8119, 2020.
- [48] Diederik P Kingma, Tim Salimans, Rafal Jozefowicz, Xi Chen, Ilya Sutskever, and Max Welling. Improved variational inference with inverse autoregressive flow. In D D Lee, M Sugiyama, U V Luxburg, I Guyon, and R Garnett, editors, *Advances in Neural Information Processing Systems 29*, pages 4743–4751. Curran Associates, Inc., 2016.
- [49] Diederik P Kingma and Max Welling. Auto-Encoding variational bayes. *arXiv preprint arXiv:1312.6114v10*, December 2013.
- [50] Alex Krizhevsky, Ilya Sutskever, and Geoffrey E Hinton. ImageNet classification with deep convolutional neural networks. In F Pereira, C J C Burges, L Bottou, and K Q Weinberger, editors, *Advances in Neural Information Processing Systems 25*, pages 1097–1105. Curran Associates, Inc., 2012.
- [51] Anders Boesen Lindbo Larsen, Søren Kaae Sønderby, Hugo Larochelle, and Ole Winther. Autoencoding beyond pixels using a learned similarity metric. In *International conference on machine learning*, pages 1558–1566. PMLR, 2016.
- [52] C Li, H Liu, C Chen, Y Pu, L Chen, and others. Alice: Towards understanding adversarial learning for joint distribution matching. *Advances in neural information processing systems*, 2017.
- [53] Chunyuan Li, Xiang Gao, Yuan Li, Baolin Peng, Xiujun Li, Yizhe Zhang, and Jianfeng Gao. Optimus: Organizing sentences via pre-trained modeling of a latent space. *arXiv preprint arXiv:2004.04092*, 2020.

- [54] Tsung-Yi Lin, Michael Maire, Serge Belongie, James Hays, Pietro Perona, Deva Ramanan, Piotr Dollár, and C Lawrence Zitnick. Microsoft coco: Common objects in context. In *European conference on computer vision*, pages 740–755. Springer, 2014.
- [55] Ziwei Liu, Ping Luo, Xiaogang Wang, and Xiaoou Tang. Deep learning face attributes in the wild. In *Proceedings of the IEEE international conference on computer vision*, pages 3730–3738, 2015.
- [56] Alireza Makhzani, Jonathon Shlens, Navdeep Jaitly, Ian Goodfellow, and Brendan Frey. Adversarial autoencoders. *arXiv preprint arXiv:1511.05644*, 2015.
- [57] Elman Mansimov, Emilio Parisotto, Jimmy Lei Ba, and Ruslan Salakhutdinov. Generating images from captions with attention. *arXiv preprint arXiv:1511.02793*, 2015.
- [58] Mehdi Mirza and Simon Osindero. Conditional generative adversarial nets. *arXiv preprint arXiv:1411.1784*, November 2014.
- [59] Gautam Mittal, Jesse Engel, Curtis Hawthorne, and Ian Simon. Symbolic music generation with diffusion models. *arXiv preprint arXiv:2103.16091*, March 2021.
- [60] Takeru Miyato, Toshiki Kataoka, Masanori Koyama, and Yuichi Yoshida. Spectral normalization for generative adversarial networks. *arXiv preprint arXiv:1802.05957*, February 2018.
- [61] Shakir Mohamed and Balaji Lakshminarayanan. Learning in implicit generative models. *arXiv preprint arXiv:1610.03483*, October 2016.
- [62] Alex Najibi. Racial Discrimination in Face Recognition Technology, 2020.
- [63] Anh Nguyen, Jeff Clune, Yoshua Bengio, Alexey Dosovitskiy, and Jason Yosinski. Plug & play generative networks: Conditional iterative generation of images in latent space. In *Proceedings of the IEEE Conference on Computer Vision and Pattern Recognition*, pages 4467–4477, 2017.
- [64] Chenhao Niu, Yang Song, Jiaming Song, Shengjia Zhao, Aditya Grover, and Stefano Ermon. Permutation invariant graph generation via score-based generative modeling. In *International Conference on Artificial Intelligence and Statistics*, pages 4474–4484. PMLR, 2020.
- [65] Mehdi Noroozi and Paolo Favaro. Unsupervised learning of visual representations by solving jigsaw puzzles. In *European conference on computer vision*, pages 69–84. Springer, 2016.
- [66] Taesung Park, Jun-Yan Zhu, Oliver Wang, Jingwan Lu, Eli Shechtman, Alexei A Efros, and Richard Zhang. Swapping autoencoder for deep image manipulation. *arXiv preprint arXiv:2007.00653*, July 2020.
- [67] Or Patashnik, Zongze Wu, Eli Shechtman, Daniel Cohen-Or, and Dani Lischinski. StyleCLIP: Text-Driven manipulation of StyleGAN imagery. *arXiv preprint arXiv:2103.17249*, March 2021.
- [68] Wei Ping, Kainan Peng, Kexin Zhao, and Zhao Song. Waveflow: A compact flow-based model for raw audio. In *International Conference on Machine Learning*, pages 7706–7716. PMLR, 2020.
- [69] Tiziano Portenier, Qiyang Hu, Attila Szabó, Siavash Arjomand Bigdeli, Paolo Favaro, and Matthias Zwicker. Faceshop: Deep sketch-based face image editing. *ACM Transactions on Graphics*, 37(4), 2018.
- [70] Alec Radford, Jong Wook Kim, Chris Hallacy, Aditya Ramesh, Gabriel Goh, Sandhini Agarwal, Girish Sastry, Amanda Askell, Pamela Mishkin, Jack Clark, Gretchen Krueger, and Ilya Sutskever. Learning transferable visual models from natural language supervision. *arXiv preprint arXiv:2103.00020*, February 2021.
- [71] Aditya Ramesh, Mikhail Pavlov, Gabriel Goh, Scott Gray, Chelsea Voss, Alec Radford, Mark Chen, and Ilya Sutskever. Zero-Shot Text-to-Image generation. *arXiv preprint arXiv:2102.12092*, February 2021.
- [72] Ali Razavi, Aaron van den Oord, and Oriol Vinyals. Generating diverse high-fidelity images with vq-vae-2. *arXiv preprint arXiv:1906.00446*, 2019.
- [73] Scott Reed, Zeynep Akata, Xinchun Yan, Lajanugen Logeswaran, Bernt Schiele, and Honglak Lee. Generative adversarial text to image synthesis. In *International Conference on Machine Learning*, pages 1060–1069. PMLR, 2016.
- [74] Danilo Jimenez Rezende and Shakir Mohamed. Variational inference with normalizing flows. *arXiv preprint arXiv:1505.05770*, May 2015.



- [75] Gareth O Roberts and Jeffrey S Rosenthal. Optimal scaling of discrete approximations to langevin diffusions. *Journal of the Royal Statistical Society: Series B (Statistical Methodology)*, 60(1):255–268, 1998.
- [76] Mihaela Rosca, Balaji Lakshminarayanan, and Shakir Mohamed. Distribution matching in variational inference. *arXiv preprint arXiv:1802.06847*, February 2018.
- [77] Yujun Shen, Jinjin Gu, Xiaoou Tang, and Bolei Zhou. Interpreting the latent space of gans for semantic face editing. In *Proceedings of the IEEE/CVF Conference on Computer Vision and Pattern Recognition*, pages 9243–9252, 2020.
- [78] Jascha Sohl-Dickstein, Eric A Weiss, Niru Maheswaranathan, and Surya Ganguli. Deep unsupervised learning using nonequilibrium thermodynamics. *arXiv preprint arXiv:1503.03585*, March 2015.
- [79] Jiaming Song and Stefano Ermon. Multi-label contrastive predictive coding. *arXiv preprint arXiv:2007.09852*, 2020.
- [80] Jiaming Song, Pratyusha Kalluri, Aditya Grover, Shengjia Zhao, and Stefano Ermon. Learning controllable fair representations. *arXiv preprint arXiv:1812.04218*, December 2018.
- [81] Jiaming Song, Chenlin Meng, and Stefano Ermon. Denoising diffusion implicit models. *arXiv preprint arXiv:2010.02502*, 2020.
- [82] Yang Song and Stefano Ermon. Generative modeling by estimating gradients of the data distribution. *arXiv preprint arXiv:1907.05600*, July 2019.
- [83] Yang Song, Jascha Sohl-Dickstein, Diederik P Kingma, Abhishek Kumar, Stefano Ermon, and Ben Poole. Score-based generative modeling through stochastic differential equations. *arXiv preprint arXiv:2011.13456*, 2020.
- [84] Hiroshi Takahashi, Tomoharu Iwata, Yuki Yamanaka, Masanori Yamada, and Satoshi Yagi. Variational autoencoder with implicit optimal priors. *Proceedings of the AAAI Conference on Artificial Intelligence*, 33(01):5066–5073, July 2019.
- [85] Ilya Tolstikhin, Olivier Bousquet, Sylvain Gelly, and Bernhard Schoelkopf. Wasserstein Auto-Encoders. *arXiv preprint arXiv:1711.01558*, November 2017.
- [86] Jakub M Tomczak and Max Welling. Improving variational auto-encoders using householder flow. *arXiv preprint arXiv:1611.09630*, 2016.
- [87] Jakub M Tomczak and Max Welling. VAE with a VampPrior. *arXiv preprint arXiv:1705.07120*, May 2017.
- [88] Arash Vahdat and Jan Kautz. NVAE: A deep hierarchical variational autoencoder. *arXiv preprint arXiv:2007.03898*, July 2020.
- [89] Aaron van den Oord, Sander Dieleman, Heiga Zen, Karen Simonyan, Oriol Vinyals, Alex Graves, Nal Kalchbrenner, Andrew Senior, and Koray Kavukcuoglu. WaveNet: A generative model for raw audio. *arXiv preprint arXiv:1609.03499*, September 2016.
- [90] Aaron van den Oord, Nal Kalchbrenner, and Koray Kavukcuoglu. Pixel recurrent neural networks. *arXiv preprint arXiv:1601.06759*, January 2016.
- [91] Aaron van den Oord, Yazhe Li, and Oriol Vinyals. Representation learning with contrastive predictive coding. *arXiv preprint arXiv:1807.03748*, July 2018.
- [92] Aaron van den Oord, Oriol Vinyals, and Koray Kavukcuoglu. Neural discrete representation learning. *arXiv preprint arXiv:1711.00937*, November 2017.
- [93] Ting-Chun Wang, Ming-Yu Liu, Jun-Yan Zhu, Andrew Tao, Jan Kautz, and Bryan Catanzaro. High-resolution image synthesis and semantic manipulation with conditional gans. In *CVPR*, 2018.
- [94] Weihao Xia, Yujun Yang, Jing-Hao Xue, and Baoyuan Wu. TediGAN: Text-Guided diverse face image generation and manipulation. 2021.
- [95] Zhe Xie, Chengxuan Liu, Yichi Zhang, Hongtao Lu, Dong Wang, and Yue Ding. Adversarial and contrastive variational autoencoder for sequential recommendation. *arXiv preprint arXiv:2103.10693*, March 2021.
- [96] Yinghao Xu, Yujun Shen, Jiapeng Zhu, Ceyuan Yang, and Bolei Zhou. Generative hierarchical features from synthesizing images. *arXiv e-prints*, pages arXiv–2007, 2020.

- [97] Jiaxuan You, Bowen Liu, Rex Ying, Vijay Pande, and Jure Leskovec. Graph convolutional policy network for Goal-Directed molecular graph generation. *arXiv preprint arXiv:1806.02473*, June 2018.
- [98] Lantao Yu, Weinan Zhang, Jun Wang, and Yong Yu. Seqgan: Sequence generative adversarial nets with policy gradient. In *Proceedings of the AAAI conference on artificial intelligence*, volume 31, 2017.
- [99] Shengjia Zhao, Jiaming Song, and Stefano Ermon. InfoVAE: Information maximizing variational autoencoders. *arXiv preprint arXiv:1706.02262*, June 2017.
- [100] Shengjia Zhao, Jiaming Song, and Stefano Ermon. Towards deeper understanding of variational autoencoding models. *arXiv preprint arXiv:1702.08658*, February 2017.
- [101] Shengjia Zhao, Jiaming Song, and Stefano Ermon. A lagrangian perspective on latent variable generative models. In *Proc. 34th Conference on Uncertainty in Artificial Intelligence*, 2018.
- [102] Jiapeng Zhu, Yujun Shen, Deli Zhao, and Bolei Zhou. In-domain gan inversion for real image editing. In *European Conference on Computer Vision*, pages 592–608. Springer, 2020.
- [103] Jiapeng Zhu, Deli Zhao, Bolei Zhou, and Bo Zhang. Lia: Latently invertible autoencoder with adversarial learning. 2019.

## A Additional Details for D2C

### A.1 Training diffusion models

We use the notations in [81] to denote the  $\alpha$  values and consider the forward diffusion model in [40]; a non-Markovian version that motivates other sampling procedures can be found in [81], but the training procedure is largely identical. We refer to the reader to these two papers for more details.

First, we define the following diffusion forward process for a series  $\{\alpha_t\}_{t=0}^T$ :

$$q(\mathbf{x}^{(\alpha_{1:T})}|\mathbf{x}^{(\alpha_0)}) := \prod_{t=1}^T q(\mathbf{x}^{(\alpha_t)}|\mathbf{x}^{(\alpha_{t-1})}), \quad (7)$$

$$q(\mathbf{x}^{(\alpha_t)}|\mathbf{x}^{(\alpha_{t-1})}) := \mathcal{N}\left(\sqrt{\frac{\alpha_t}{\alpha_{t-1}}}\mathbf{x}^{(\alpha_{t-1})}, \left(1 - \frac{\alpha_t}{\alpha_{t-1}}\right)\mathbf{I}\right), \quad (8)$$

and from standard derivations for Gaussian we have that:

$$q(\mathbf{x}^{(\alpha_{t-1})}|\mathbf{x}^{(\alpha_t)}, \mathbf{x}^{(\alpha_0)}) = \mathcal{N}\left(\underbrace{\frac{\sqrt{\alpha_{t-1}-\alpha_t}}{1-\alpha_t}\mathbf{x}^{(\alpha_0)} + \frac{\alpha_t(1-\alpha_{t-1})}{\alpha_{t-1}(1-\alpha_t)}\mathbf{x}^{(\alpha_t)}}_{\tilde{\mu}(\mathbf{x}^{(\alpha_t)}, \mathbf{x}^{(\alpha_0)}; \alpha_t, \alpha_{t-1})}, \frac{1-\alpha_{t-1}}{1-\alpha_t}\left(1 - \frac{\alpha_t}{\alpha_{t-1}}\right)\mathbf{I}\right). \quad (9)$$

As a variational approximation to the above, [40] considered a specific type of  $p_\theta(\mathbf{x}^{(\alpha_{t-1})}|\mathbf{x}^{(\alpha_t)})$ :

$$p_\theta(\mathbf{x}^{(\alpha_{t-1})}|\mathbf{x}^{(\alpha_t)}) = \mathcal{N}\left(\mu_\theta(\mathbf{x}^{(\alpha_t)}; \alpha_t, \alpha_{t-1}), (\sigma^{(\alpha_t)})^2\mathbf{I}\right), \quad (10)$$

where  $\mu_\theta$  and  $\sigma^{(\alpha_t)}$  are parameters, and we remove the superscript of  $p_\theta$  to indicate that there are no additional discretization steps in between (the sampling process is explicitly defined). Then, we have the standard variational objective as follows:

$$\begin{aligned} L &:= \mathbb{E}_q \left[ \log q(\mathbf{x}^{(\alpha_T)}|\mathbf{x}^{(\alpha_0)}) + \sum_{t=2}^T \log q(\mathbf{x}^{(\alpha_{t-1})}|\mathbf{x}^{(\alpha_t)}, \mathbf{x}^{(\alpha_0)}) - \sum_{t=1}^T \log p_\theta^{(\alpha_t, \alpha_{t-1})}(\mathbf{x}^{(\alpha_{t-1})}|\mathbf{x}^{(\alpha_t)}) \right] \\ &\equiv \mathbb{E}_q \left[ \sum_{t=2}^T \underbrace{D_{\text{KL}}(q(\mathbf{x}^{(\alpha_{t-1})}|\mathbf{x}^{(\alpha_t)}, \mathbf{x}^{(\alpha_0)})||p_\theta(\mathbf{x}^{(\alpha_{t-1})}|\mathbf{x}^{(\alpha_t)}))}_{L_{t-1}} - \log p_\theta(\mathbf{x}^{(\alpha_0)}|\mathbf{x}^{(\alpha_1)}) \right], \end{aligned}$$

where  $\equiv$  denotes “equal up to a constant that does not depend on  $\theta$ ” and each  $L_{t-1}$  is a KL divergence between two Gaussian distributions. Let us assume that the standard deviation of  $p_\theta(\mathbf{x}^{(\alpha_{t-1})}|\mathbf{x}^{(\alpha_t)})$  is equal to that of  $q(\mathbf{x}^{(\alpha_{t-1})}|\mathbf{x}^{(\alpha_t)}, \mathbf{x}^{(\alpha_0)})$ , which we denote as  $\sigma^{(\alpha_t)}$ . And thus:

$$L_{t-1} = \mathbb{E}_q \left[ \frac{1}{2(\sigma^{(\alpha_t)})^2} \|\mu_\theta(\mathbf{x}^{(\alpha_t)}; \alpha_t, \alpha_{t-1}) - \tilde{\mu}(\mathbf{x}^{(\alpha_t)}, \mathbf{x}^{(\alpha_0)}; \alpha_t, \alpha_{t-1})\|_2^2 \right]. \quad (11)$$

With a particular reparametrization from  $\mu_\theta$  to  $\epsilon_\theta$  (which tries to model the noise vector at  $\alpha_t$ ):

$$\mu_\theta(\mathbf{x}^{(\alpha_t)}; \alpha_t, \alpha_{t-1}) = \sqrt{\frac{\alpha_{t-1}}{\alpha_t}} \left( \mathbf{x}^{(\alpha_t)} - \frac{\sqrt{\alpha_{t-1}-\alpha_t}}{\sqrt{(1-\alpha_t)\alpha_t}} \cdot \epsilon_\theta(\mathbf{x}^{(\alpha_t)}; \alpha_t) \right), \quad (12)$$

the objective function can be simplified to:

$$L_{t-1} = \mathbb{E}_{\mathbf{x}_0, \epsilon} \left[ \frac{(\alpha_{t-1} - \alpha_t)}{2(\sigma^{(\alpha_t)})^2(1 - \alpha_t)\alpha_t} \|\epsilon - \epsilon_\theta(\mathbf{x}^{(\alpha_t)}; \alpha_t, \alpha_{t-1})\|_2^2 \right] \quad (13)$$

where  $\mathbf{x}^{(\alpha_t)} = \sqrt{\alpha_t}\mathbf{x}_0 + \sqrt{1-\alpha_t}\epsilon$ . Intuitively, this is a weighted sum of mean-square errors between the noise model  $\epsilon_\theta$  and the actual noise  $\epsilon$ . Other weights can also be derived with different forward processes that are non-Markovian [81], and in practice, setting the weights to 1 is observed to achieve decent performance for image generation.

## A.2 DDIM sampling procedure

In this section, we discuss the detailed sampling procedure from  $\mathbf{x}^{(0)} \sim \mathcal{N}(0, \mathbf{I})$  (which is the distribution with “all noise”<sup>7</sup>) to  $\mathbf{x}^{(1)}$  (which is the model distribution with “no noise”). More specifically, we discuss a deterministic sampling procedure, which casts the generation procedure as an implicit model [81]. Compared to other procedures (such as the one in DDPM [40]), this has the advantage of better sample quality when few steps are allowed to produce each sample, as well as a near-invertible mapping between  $\mathbf{x}^{(0)}$  and  $\mathbf{x}^{(1)}$ . We describe this procedure in Algorithm 2, where we can choose different series of  $\alpha$  to control how many steps (and through which steps) we wish to draw a sample. The DDIM sampling procedure corresponds to a particular discretization to an ODE, we note that it is straightforward to also define the sampling procedure between any two  $\alpha$  values. Similarly, given an observation  $\mathbf{x}^{(1)}$  we can obtain the corresponding latent code  $\mathbf{x}^{(0)}$  by sampling running Algorithm 2 with the sequence of  $\alpha$  reversed.

---

### Algorithm 2 Sampling with the DDIM procedure

---

- 1: **Input:** non-increasing series  $\{\alpha_t\}_{t=0}^T$  with  $\alpha_T = 0$  and  $\alpha_0 = 1$ .
- 2: Sample  $\mathbf{x}^{(1)} \sim \mathcal{N}(0, \mathbf{I})$ .
- 3: **for**  $k \leftarrow T$  to 1 **do**
- 4:   Update  $\mathbf{x}^{(\alpha_{t-1})}$  from  $\mathbf{x}^{(\alpha_t)}$  such that

$$\sqrt{\frac{1}{\alpha_{t-1}}} \mathbf{x}^{(\alpha_{t-1})} = \sqrt{\frac{1}{\alpha_t}} \mathbf{x}^{(\alpha_t)} + \left( \sqrt{\frac{1 - \alpha_{t-1}}{\alpha_{t-1}}} - \sqrt{\frac{1 - \alpha_t}{\alpha_t}} \right) \cdot \epsilon_\theta(\mathbf{x}^{(\alpha_t)}; \alpha_t)$$

- 5: **end for**
  - 6: **Output**  $\mathbf{x}^{(0)}$ .
- 

## A.3 Contrastive representation learning

In contrastive representation learning, the goal is to distinguish a *positive* pair  $(\mathbf{y}, \mathbf{w}) \sim p(\mathbf{y}, \mathbf{w})$  from  $(m - 1)$  *negative* pairs  $(\mathbf{y}, \bar{\mathbf{w}}) \sim p(\mathbf{y})p(\mathbf{w})$ . In our context, the positive pairs are representations from the same image, and negative pairs are representations from different images; these images are pre-processed with strong data augmentations [14] to encourage rich representations. With two random, independent data augmentation procedures defined as  $\text{aug}_1$  and  $\text{aug}_2$ , we define  $p(\mathbf{y}, \mathbf{w})$  and  $p(\mathbf{y})p(\mathbf{w})$  via the following sampling procedure:

$$\begin{aligned} (\mathbf{y}, \mathbf{w}) \sim p(\mathbf{y}, \mathbf{w}) : & \mathbf{y} \sim q_\phi(\mathbf{z}^{(1)} | \text{aug}_1(\mathbf{x})), \mathbf{w} \sim q_\phi(\mathbf{z}^{(1)} | \text{aug}_2(\mathbf{x})), \mathbf{x} \sim p_{\text{data}}(\mathbf{x}), \\ (\mathbf{y}, \mathbf{w}) \sim p(\mathbf{y})p(\mathbf{w}) : & \mathbf{y} \sim q_\phi(\mathbf{z}^{(1)} | \text{aug}_1(\mathbf{x}_1)), \mathbf{w} \sim q_\phi(\mathbf{z}^{(1)} | \text{aug}_2(\mathbf{x}_2)), \mathbf{x}_1, \mathbf{x}_2 \sim p_{\text{data}}(\mathbf{x}). \end{aligned}$$

For a batch of  $n$  positive pairs  $\{(\mathbf{y}_i, \mathbf{w}_i)\}_{i=1}^n$ , the contrastive predictive coding (CPC, [91]) objective is defined as:

$$L_{\text{CPC}}(g; q_\phi) := \mathbb{E} \left[ \frac{1}{n} \sum_{i=1}^n \log \frac{m \cdot g(\mathbf{y}_i, \mathbf{w}_i)}{g(\mathbf{y}_i, \mathbf{w}_i) + \sum_{j=1}^{m-1} g(\mathbf{y}_i, \bar{\mathbf{w}}_{i,j})} \right] \quad (14)$$

for some positive critic function  $g : \mathcal{Y} \times \mathcal{Z} \rightarrow \mathbb{R}_+$ , where the expectation is taken over  $n$  positive pairs  $(\mathbf{y}_i, \mathbf{w}_i) \sim p(\mathbf{y}, \mathbf{w})$  and  $n(m - 1)$  negative pairs  $(\mathbf{y}_i, \bar{\mathbf{w}}_{i,j}) \sim p(\mathbf{y})p(\mathbf{w})$ . Another interpretation to CPC is that it performs  $m$ -way classification where the ground truth label is assigned to the positive pair. The representation learner  $q_\phi$  then aims to maximize the CPC objective, or to minimize the following objective:

$$-L_C(q_\phi) := \min_g -L_{\text{CPC}}(g; q_\phi), \quad (15)$$

Different specific implementations, such as MoCo [35, 15, 17] and SimCLR [14] can all be treated as specific implementations of this objective function. In this paper, we considered using MoCo-v2 [14] as our implementation for  $L_C$  objective; in principle, other implementations to CPC can also be integrated into D2C as well.

---

<sup>7</sup>Technically, the maximum noise level  $\alpha_T$  should have  $\alpha_T \rightarrow 0$  but not equal to 0, but we can approximate the distribution of  $\mathbf{x}^{(\alpha_T)}$  with that of  $\mathbf{x}^{(0)}$  arbitrarily well in practice.

#### A.4 Training D2C

In Algorithm 3, we describe a high-level procedure that trains the D2C model; we note that this procedure does not have any adversarial components. On the high-level, this is the integration of three objectives: the reconstruction objective via the autoencoder, the diffusion objective over the latent space, and the contrastive objective over the latent space. In principle, the [reconstruction], [contrastive], and [diffusion] components can be optimized jointly or separately; we observe that normalizing the latent  $\mathbf{z}^{(1)}$  with a global mean and standard deviation before applying the diffusion objective helps learning the diffusion model with a fixed  $\alpha$  series.

---

##### Algorithm 3 Training D2C

---

**Input:** Data distribution  $p_{\text{data}}$ .  
**while** training **do**

###### [Draw samples with data augmentation]

Draw  $m$  samples  $\mathbf{x}_{0:m-1} \sim p_{\text{data}}(\mathbf{x})$ .  
 Draw  $(m + 1)$  data augmentations  $\text{aug}_0, \dots, \text{aug}_{m-1}$  and  $\overline{\text{aug}}_0$ .  
**for**  $i \leftarrow 0$  to  $m - 1$  **do**  
     Draw  $\mathbf{z}_i^{(1)} \sim q_\phi(\mathbf{z}^{(1)} | \text{aug}_i(\mathbf{x}))$ .  
**end for**  
 Draw  $\bar{\mathbf{z}}_0^{(1)} \sim q_\phi(\mathbf{z}^{(1)} | \overline{\text{aug}}_0(\mathbf{x}))$ .

###### [Reconstruction]

Reconstruct  $\mathbf{x}_0 \sim p_\theta(\mathbf{x} | \mathbf{z}_0^{(1)})$   
 Minimize  $L_{\text{recon}} = -\log p_\theta(\mathbf{x} | \mathbf{z}_0^{(1)})$  over  $\theta$  and  $\phi$  with gradient descent.

###### [Contrastive]

Define a classification task: assign label 1 to  $(\mathbf{z}_0^{(1)}, \bar{\mathbf{z}}_0^{(1)})$  and label 0 to  $(\mathbf{z}_0^{(1)}, \mathbf{z}_i^{(1)})$  for  $i \neq 0$ .  
 Define  $L_{\text{CPC}}(g; q_\phi)$  as the loss to minimize for the above task, with  $g$  as the classifier.  
 Define  $\hat{g}$  as a minimizer to the classifier objective  $L_{\text{CPC}}(g; q_\phi)$ .  
 Minimize  $L_{\text{CPC}}(\hat{g}; q_\phi)$  over  $\phi$  with gradient descent.

###### [Diffusion]

Sample  $\epsilon \sim \mathcal{N}(0, I)$ ,  $t \sim \text{Uniform}(1, \dots, T)$ .  
 Define  $\mathbf{z}_0^{(\alpha_t)} = \sqrt{\alpha_t} \mathbf{z}_0^{(0)} + \sqrt{1 - \alpha_t} \epsilon$ .  
 Minimize  $\|\epsilon - \epsilon_\theta(\mathbf{z}_0^{(\alpha_t)}; \alpha_t)\|_2^2$  over  $\theta$  with gradient descent.

**end while**

---

#### A.5 Few-shot conditional generation

In order to perform few-shot conditional generation, we need to implement line 4 in Algorithm 1, where an unnormalized (energy-based) model is defined over the representations. After we have defined the energy-based model, we implement a procedure to draw samples from this unnormalized model. We note that our approach (marked in teal boxes) is only one way of drawing valid samples, and not necessarily the optimal one. Furthermore, these implementations can also be done over the image space (which is the case for DDIM-I), which may costs more to compute than over the latent space since more layers are needed in a neural network to process it.

For generation from labels, we would define the energy-based model over latents as the product of two components: the first is the “prior” over  $\mathbf{z}^{(1)}$  as defined by the diffusion model and the second is the “likelihood” of the label  $c$  being true given the latent variable  $\mathbf{z}^{(1)}$ . This places high energy values to the latent variables that are likely to occur under the diffusion prior (so generated images are likely to have high quality) as well as latent variables that have the label  $c$ . To sample from this energy-based model, we perform a rejection sampling procedure, where we reject latent samples from the diffusion model that have low discriminator values. This procedure is describe in Algorithm 4.



---

**Algorithm 4** Generate from labels

---

**Input** model  $r_\psi(\mathbf{c}|\mathbf{z}^{(1)})$ , target label  $\mathbf{c}$ .

**Define latent energy-based model**

$$E(\hat{\mathbf{z}}^{(1)}) = r_\psi(\mathbf{c}|\hat{\mathbf{z}}^{(1)}) \cdot p_\theta^{(1)}(\hat{\mathbf{z}}^{(1)})$$

**Sample from  $E(\hat{\mathbf{z}}^{(1)})$**

**while** True **do**

    Sample  $\hat{\mathbf{z}}^{(1)} \sim p_\theta^{(1)}(\hat{\mathbf{z}}^{(1)})$ ;

    Sample  $u \sim \text{Uniform}(0, 1)$ ;

**If**  $u < r_\psi(\mathbf{c}|\hat{\mathbf{z}}^{(1)})$  **then** break.

**end while**

**Output**  $\hat{\mathbf{x}} \sim p_\theta(\mathbf{x}|\hat{\mathbf{z}}^{(1)})$ .

---

For generation from manipulation constraints, we need to further define a prior that favors closeness to the given latent variable so that the manipulated generation is close to the given image except for the label  $\mathbf{z}$ . If the latent variable for the original image is  $\mathbf{z}^{(1)} \sim q_\phi(\mathbf{z}^{(1)}|\mathbf{x})$ , then we define the closeness via the L2 distance between the it and the manipulated latent. We obtain the energy-based model by multiplying this with the diffusion “prior” and the classifier “likelihood”. Then, we approximately draw samples from this energy by taking a gradient step from the original latent value  $\mathbf{z}^{(1)}$  and then regularizing it with the diffusion prior; this is described in Algorithm 5. A step size  $\eta$ , diffusion noise magnitude  $\alpha$ , and the diffusion steps from  $\alpha$  to 1 are chosen as hyperparameters. We choose one  $\eta$  for each attribute,  $\alpha \approx 0.9$ , and number of discretization steps to be 5<sup>8</sup>; we tried  $\alpha \in [0.65, 0.9]$  and found that our results are not very sensitive to values within this range. We list the  $\eta$  values for each attribute (details in Appendix C).

We note that a more principled approach is to take gradient with respect to the entire energy function (*e.g.*, for Langevin dynamics), where the gradient over the DDIM can be computed with instantaneous change-of-variables formula [13]; we observe that our current version is computationally efficient enough to perform well.

---

**Algorithm 5** Generate from manipulation constraints

---

**Input** model  $r_\psi(\mathbf{c}|\mathbf{z}^{(1)})$ , target label  $\mathbf{c}$ , original image  $\mathbf{x}$ .

Acquire latent  $\mathbf{z}^{(1)} \sim q_\phi(\mathbf{z}^{(1)}|\mathbf{x})$ ;

Fit a model  $r_\psi(\mathbf{c}|\mathbf{z}^{(1)})$  over  $\{(\mathbf{z}_i^{(1)}, \mathbf{c}_i)\}_{i=1}^n$

**Define latent energy-based model**

$$E(\hat{\mathbf{z}}^{(1)}) = r_\psi(\mathbf{c}|\hat{\mathbf{z}}^{(1)}) \cdot p_\theta^{(1)}(\hat{\mathbf{z}}^{(1)}) \cdot \|\mathbf{z}^{(1)} - \hat{\mathbf{z}}^{(1)}\|_2^2$$

**Sample from  $E(\hat{\mathbf{z}}^{(1)})$  (approximate)**

Choose hyperparameters  $\eta > 0, \alpha \in (0, 1)$ .

Take a gradient step  $\tilde{\mathbf{z}}^{(1)} \leftarrow \mathbf{z}^{(1)} + \eta \nabla_{\mathbf{z}} r_\psi(\mathbf{c}|\mathbf{z})|_{\mathbf{z}=\mathbf{z}^{(1)}}$ .

Add noise  $\tilde{\mathbf{z}}^{(\alpha)} \leftarrow \sqrt{\alpha} \tilde{\mathbf{z}}^{(1)} + \sqrt{1 - \alpha} \epsilon$ .

Sample  $\hat{\mathbf{z}}^{(1)} \sim p_\theta^{(\alpha, 1)}(\mathbf{z}^{(1)}|\tilde{\mathbf{z}}^{(\alpha)})$  with DDIM, *i.e.*, use the diffusion prior to “denoise”.

**Output**  $\hat{\mathbf{x}} \sim p_\theta(\mathbf{x}|\hat{\mathbf{z}}^{(1)})$ .

---

<sup>8</sup>The results are not particularly sensitive to how the discretization steps are chosen. For example, one can take  $0.9 \rightarrow 0.92 \rightarrow 0.96 \rightarrow 0.98 \rightarrow 0.99 \rightarrow 1$ .

## B Formal Statements and Proofs

### B.1 Relationship to maximum likelihood

**Theorem 1.** (informal) For any valid  $\{\alpha_i\}_{i=0}^T$ , there exists some weights  $\hat{w} : \{\alpha_i\}_{i=1}^T \rightarrow \mathbb{R}_+$  for the diffusion objective such that  $-L_{D2}$  is a variational lower bound to the log-likelihood, i.e.,

$$-L_{D2}(\theta, \phi; \hat{w}) \leq \mathbb{E}_{p_{\text{data}}}[\log p_{\theta}(\mathbf{x})], \quad (6)$$

where  $p_{\theta}(\mathbf{x}) := \mathbb{E}_{\mathbf{z}_0 \sim p^{(0)}(\mathbf{z}^{(0)})}[p_{\theta}(\mathbf{x}|\mathbf{z}^{(0)})]$  is the marginal probability of  $\mathbf{x}$  under the D2C model.

**Theorem 3.** (formal) Suppose that  $\mathbf{x} \in \mathbb{R}^d$ . For any valid  $\{\alpha_i\}_{i=0}^T$ , let  $\hat{w}$  satisfy:

$$\forall t \in [2, \dots, T], \quad \hat{w}(\alpha_t) = \frac{(1 - \alpha_t)\alpha_{t-1}}{2(1 - \alpha_{t-1})^2\alpha_t} \quad (16)$$

$$\hat{w}(\alpha_1) = \frac{1 - \alpha_1}{2(2\pi)^d\alpha_1} \quad (17)$$

then:

$$-L_{D2}(\theta, \phi; \hat{w}) + H(q_{\phi}(\mathbf{z}^{(1)}|\mathbf{x})) \leq \mathbb{E}_{p_{\text{data}}}[\log p_{\theta}(\mathbf{x})] \quad (18)$$

where  $p_{\theta}(\mathbf{x}) := \mathbb{E}_{\mathbf{z}_0 \sim p^{(0)}(\mathbf{z}^{(0)})}[p_{\theta}(\mathbf{x}|\mathbf{z}^{(0)})]$  is the marginal probability of  $\mathbf{x}$  under the D2C model.

*Proof.* First, we have that:

$$\mathbb{E}_{p_{\text{data}}(\mathbf{x})}[\log p_{\theta}(\mathbf{x})] = \mathbb{E}_{p_{\text{data}}(\mathbf{x})} \left[ \log \sum_{\mathbf{z}^{(1)}} p_{\theta}(\mathbf{x}|\mathbf{z}^{(1)}) p_{\theta}(\mathbf{z}^{(1)}) \right] \quad (19)$$

$$\geq \mathbb{E}_{p_{\text{data}}(\mathbf{x}), q_{\phi}(\mathbf{z}^{(1)}|\mathbf{x})} [\log p_{\theta}(\mathbf{x}|\mathbf{z}^{(1)}) + \log p_{\theta}(\mathbf{z}^{(1)}) - \log q_{\phi}(\mathbf{z}^{(1)}|\mathbf{x})] \quad (20)$$

$$= \mathbb{E}_{p_{\text{data}}(\mathbf{x}), q_{\phi}(\mathbf{z}^{(1)}|\mathbf{x})} [\log p_{\theta}(\mathbf{x}|\mathbf{z}^{(1)}) - D_{\text{KL}}(q_{\phi}(\mathbf{z}^{(1)}|\mathbf{x}) \| p_{\theta}(\mathbf{z}^{(1)}))]. \quad (21)$$

where we use Jensen's inequality here. Compared with the objective for D2:

$$-L_{D2}(\theta, \phi; w) := \mathbb{E}_{\mathbf{x} \sim p_{\text{data}}, \mathbf{z}^{(1)} \sim q_{\phi}(\mathbf{z}^{(1)}|\mathbf{x})} [\log p(\mathbf{x}|\mathbf{z}^{(1)}) - \ell_{\text{diff}}(\mathbf{z}^{(1)}; w, \theta)], \quad (22)$$

and it is clear the proof is complete if we show that:

$$H(q_{\phi}(\mathbf{z}^{(1)}|\mathbf{x})) - \mathbb{E}_{\mathbf{z}^{(1)} \sim q_{\phi}(\mathbf{z}^{(1)}|\mathbf{x})} [\ell_{\text{diff}}(\mathbf{z}^{(1)}; \hat{w}, \theta)] \quad (23)$$

$$\leq -D_{\text{KL}}(q_{\phi}(\mathbf{z}^{(1)}|\mathbf{x}) \| p_{\theta}(\mathbf{z}^{(1)})) \quad (24)$$

$$= H(q_{\phi}(\mathbf{z}^{(1)}|\mathbf{x})) + \mathbb{E}_{\mathbf{z}^{(1)} \sim q_{\phi}(\mathbf{z}^{(1)}|\mathbf{x})} [\log p_{\theta}(\mathbf{z}^{(1)})] \quad (25)$$

or equivalently:

$$\mathbb{E}_{\mathbf{z}^{(1)} \sim q_{\phi}(\mathbf{z}^{(1)}|\mathbf{x})} [\ell_{\text{diff}}(\mathbf{z}^{(1)}; \hat{w}, \theta)] \leq \mathbb{E}_{\mathbf{z}^{(1)} \sim q_{\phi}(\mathbf{z}^{(1)}|\mathbf{x})} [\log p_{\theta}(\mathbf{z}^{(1)})] \quad (26)$$

Let us apply variational inference with an inference model  $q(\mathbf{z}^{(\alpha_{1:T})}|\mathbf{z}^{(1)})$  where  $\alpha_0 = 1$  and  $\alpha_T = 0$ :

$$\begin{aligned} \mathbb{E}_{\mathbf{z}^{(1)} \sim q_{\phi}(\mathbf{z}^{(1)}|\mathbf{x})} [\log p_{\theta}(\mathbf{z}^{(1)})] &= \mathbb{E}_{\mathbf{z}^{(1)} \sim q_{\phi}(\mathbf{z}^{(1)}|\mathbf{x})} [\log \sum_{\mathbf{z}} (p_{\theta}(\mathbf{z}^{(\alpha_T)}) \prod_{t=1}^T p_{\theta}(\mathbf{z}^{(\alpha_{t-1})}|\mathbf{z}^{(\alpha_t)}))] \\ &\geq \mathbb{E}_{\mathbf{z}^{(\alpha_0:T)}} [\log p_{\theta}(\mathbf{z}^{(\alpha_T)}) + \sum_{t=1}^T \log p_{\theta}(\mathbf{z}^{(\alpha_{t-1})}|\mathbf{z}^{(\alpha_t)}) - \log q(\mathbf{z}^{(\alpha_{1:T})}|\mathbf{z}^{(\alpha_0)})] \end{aligned} \quad (27)$$

$$\begin{aligned} &\geq \mathbb{E}_{\mathbf{z}^{(\alpha_0:T)}} \left[ \log p_{\theta}(\mathbf{z}^{(\alpha_T)}) - \log q(\mathbf{z}^{(\alpha_T)}|\mathbf{z}^{(\alpha_0)}) \right. \\ &\quad \left. - \sum_{t=2}^T \underbrace{D_{\text{KL}}(q(\mathbf{z}^{(\alpha_{t-1})}|\mathbf{z}^{(\alpha_t)}, \mathbf{z}^{(\alpha_0)}) \| p_{\theta}(\mathbf{z}^{(\alpha_{t-1})}|\mathbf{z}^{(\alpha_t)}))}_{L_{t-1}} + \log p_{\theta}(\mathbf{z}^{(\alpha_0)}|\mathbf{z}^{(\alpha_1)}) \right] \end{aligned} \quad (28)$$

where we remove the superscript of  $p_{\theta}$  to indicate that there are no intermediate discretization steps between  $\alpha_{t-1}$  and  $\alpha_t$ . Now, for  $t \geq 2$ , let us consider  $p_{\theta}$  and  $q_{\phi}$  with the form in Equations 9

and 10 respectively, which are both Gaussian distributions (restrictions to  $p_\theta$  will still give lower bounds). Then we can model the standard deviation of  $p_\theta(\mathbf{x}^{(\alpha_{t-1})}|\mathbf{x}^{(\alpha_t)})$  to be equal to that of  $q(\mathbf{x}^{(\alpha_{t-1})}|\mathbf{x}^{(\alpha_t)}, \mathbf{x}^{(\alpha_0)})$ . Under this formulation, the KL divergence for  $L_{t-1}$  is just one between two Gaussians with the same standard deviations and is a weighted Euclidean distance between the means. Using the derivation from Equation (11) to Equation (13), we have that:

$$L_{t-1} = \mathbb{E}_{\mathbf{z}_0, \epsilon} \left[ \frac{(1 - \alpha_t)\alpha_{t-1}}{2(1 - \alpha_{t-1})^2\alpha_t} \|\epsilon - \epsilon_\theta(\mathbf{z}^{(\alpha_t)}; \alpha_t, \alpha_{t-1})\|_2^2 \right] \quad (29)$$

which gives us the weights for  $\hat{w}$  for  $\alpha_{2:T}$ . For  $p_\theta(\mathbf{z}^{(\alpha_0)}|\mathbf{z}^{(\alpha_1)})$  let us model it to be a Gaussian with mean

$$\mu_\theta(\mathbf{z}^{(\alpha_1)}; \alpha_1, \alpha_0) = \frac{\mathbf{z}^{(\alpha_1)} - \sqrt{1 - \alpha_t}\epsilon_\theta(\mathbf{z}^{(\alpha_1)}; \alpha_1, \alpha_0)}{\sqrt{\alpha_1}}$$

and standard deviation  $1/\sqrt{2\pi}$  (chosen such that normalization constant is 1). Thus, with

$$\mathbf{z}^{(0)} = \frac{\mathbf{z}^{(\alpha_1)} - \sqrt{1 - \alpha_t}\epsilon}{\sqrt{\alpha_1}}$$

we have that:

$$\log p_\theta(\mathbf{z}^{(\alpha_0)}|\mathbf{z}^{(\alpha_1)}) = \frac{1 - \alpha_1}{2(2\pi)^d\alpha_1} \|\epsilon - \epsilon_\theta(\mathbf{z}^{(\alpha_1)}; \alpha_1, \alpha_0)\|_2^2 \quad (30)$$

which gives us the weight of  $\hat{w}$  for  $\alpha_1$ . Furthermore:

$$\mathbb{E}_{\mathbf{z}^{(\alpha_0:T)}} [\log p_\theta(\mathbf{z}^{(\alpha_T)}) - q(\mathbf{z}^{(\alpha_T)}|\mathbf{z}^{(\alpha_0)})] = 0 \quad (31)$$

because  $\mathbf{z}^{(\alpha_T)} \sim \mathcal{N}(0, \mathbf{I})$  for both  $p_\theta$  and  $q$ . Therefore, we have that:

$$\mathbb{E}_{\mathbf{z}^{(1)} \sim q_\phi(\mathbf{z}^{(1)}|\mathbf{x})} [\ell_{\text{diff}}(\mathbf{z}^{(1)}; \hat{w}, \theta)] \leq \mathbb{E}_{\mathbf{z}^{(1)} \sim q_\phi(\mathbf{z}^{(1)}|\mathbf{x})} [\log p_\theta(\mathbf{z}^{(1)})] \quad (32)$$

which completes the proof.  $\square$

## B.2 D2 models address latent posterior mismatch in VAEs

**Theorem 2.** (informal) Let  $p_\theta(\mathbf{z}) = \mathcal{N}(0, 1)$ . For any  $\epsilon > 0$ , there exists a distribution  $q_\phi(\mathbf{z})$  with an  $(\epsilon, 0.49)$ -prior hole, such that  $D_{\text{KL}}(q_\phi\|p_\theta) \leq \log 2^9$  and  $W_2(q_\phi, p_\theta) < \gamma$  for any  $\gamma > 0$ , where  $W_2$  is the 2-Wasserstein distance.

**Theorem 4.** (formal) Let  $p_\theta(\mathbf{z}) = \mathcal{N}(0, \mathbf{I})$  where  $\mathbf{z} \in \mathbb{R}^d$ . For any  $\epsilon > 0, \delta < 0.5$ , there exists a distribution  $q_\phi(\mathbf{z})$  with an  $(\epsilon, \delta)$ -prior hole, such that  $D_{\text{KL}}(q_\phi\|p_\theta) \leq \log 2$  and  $W_2(q_\phi, p_\theta) < \gamma$  for any  $\gamma > 0$ , where  $W_2$  is the 2-Wasserstein distance.

*Proof.* Let us define a function  $f : \mathbb{R}_{\geq 0} \rightarrow [0, 1]$  such that for any Euclidean ball  $B(0, R)$  centered at 0 with radius  $R$ :

$$f(R) := \int_{B(0, R)} p_\theta(\mathbf{z}) d\mathbf{z}, \quad (33)$$

i.e.,  $f(R)$  measures the probability mass of the Gaussian distribution  $p_\theta(\mathbf{z})$  within  $B(0, R)$ . As  $df/dR > 0$  for  $R > 0$ ,  $f$  is invertible.

Now we shall construct  $q_\phi(\mathbf{z})$ . First, let  $q_\phi(\mathbf{z}) = p_\theta(\mathbf{z})$  whenever  $\|\mathbf{z}\|_2 \geq f^{-1}(2\delta)$ ; then for any  $n$ , we can find a sequence  $\{r_0, r_1, \dots, r_{2n}\}$  such that:

$$r_0 = 0, \quad r_{2n} = f^{-1}(2\delta), \quad f(r_i) - f(r_{i-1}) = f^{-1}(2\delta)\delta/n \text{ for all } i \in \{1, \dots, 2n\}, \quad (34)$$

Intuitively, we find  $2n$  circles with radii  $\{r_0, \dots, r_{2n}\}$  whose masses measured by  $p_\theta(\mathbf{z})$  is an arithmetic progression  $\{0, \delta/2n, \dots, 2\delta\}$ . We then define  $q_\phi(\mathbf{z})$  for  $\|\mathbf{z}\| < f^{-1}(2\delta)$  as follows:

$$q_\phi(\mathbf{z}) = \begin{cases} 2 \cdot p_\theta(\mathbf{z}) & \text{if } \|\mathbf{z}\| \in \bigcup_{k=0}^{n-1} [r_{2k}, r_{2k+1}) \\ 0 & \text{otherwise} \end{cases} \quad (35)$$

<sup>9</sup>This is reasonably low for realistic VAE models (NVAE [88] reports a KL divergence of around 2810 nats).

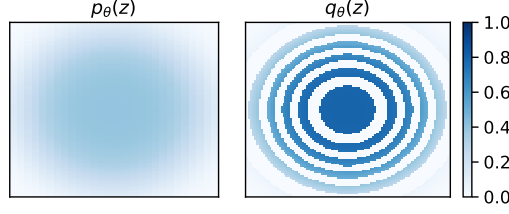


Figure 6: Illustration of the construction in 2d. When we use more rings, the prior hole and upper bound of KL divergence are constant but the upper bound of Wasserstein distance decreases.

Intuitively,  $q_\phi$  is defined by moving all the mass from ring  $(2k + 1)$  to ring  $2k$ . Note that this  $q_\phi(\mathbf{z})$  is a valid probability distribution because:

$$\int_{\mathbb{R}^d} q_\phi(\mathbf{z}) d\mathbf{z} = \int_{B(0, f^{-1}(2\delta))} q_\phi(\mathbf{z}) d\mathbf{z} + \int_{B^c(0, f^{-1}(2\delta))} q_\phi(\mathbf{z}) d\mathbf{z} \quad (36)$$

$$= 2 \int_{B(0, f^{-1}(2\delta))} p_\theta(\mathbf{z}) \mathbb{I} \left( \|\mathbf{z}\| \in \bigcup_{i=0}^{n-1} [r_{2k}, r_{2k+1}) \right) d\mathbf{z} + \int_{B^c(0, f^{-1}(2\delta))} p_\theta(\mathbf{z}) d\mathbf{z} \quad (37)$$

$$= \int_{B(0, f^{-1}(2\delta))} p_\theta(\mathbf{z}) d\mathbf{z} + \int_{B^c(0, f^{-1}(2\delta))} p_\theta(\mathbf{z}) d\mathbf{z} = 1 \quad (38)$$

Next, we validate that  $q_\phi$  satisfies our constraints in the statement.

**Prior hole** Apparently, if we choose  $\mathcal{S} = \bigcup_{k=0}^{n-1} [r_{2k+1}, r_{2k+2})$ , then  $\int_{\mathcal{S}} p_\theta(\mathbf{z}) d\mathbf{z} = \delta$  and  $\int_{\mathcal{S}} q_\phi(\mathbf{z}) d\mathbf{z} = 0$ ; so  $\mathcal{S}$  instantiates a  $(\epsilon, \delta)$ -prior hole.

**KL divergence** We note that  $q_\phi(\mathbf{z}) \leq 2p_\theta(\mathbf{z})$  is true for all  $\mathbf{z}$ , so

$$D_{\text{KL}}(q_\phi(\mathbf{z}) \| p_\theta(\mathbf{z})) = \mathbb{E}_{\mathbf{z} \sim q_\phi(\mathbf{z})} [\log q_\phi(\mathbf{z}) - \log p_\theta(\mathbf{z})] \leq \log 2.$$

**2 Wasserstein Distance** We use the Monge formulation:

$$W_2(q_\phi(\mathbf{z}), 2p_\theta(\mathbf{z})) = \min_{T: q_\phi = T_\# p_\theta} \int_{\mathbb{R}^d} \|\mathbf{z} - T(\mathbf{z})\|_2^2 p_\theta(\mathbf{z}) d\mathbf{z} \quad (39)$$

where  $T$  is any transport map from  $p_\theta$  to  $q_\phi$ . Consider the transport map  $\hat{T}$  such that:

$$\hat{T}(\mathbf{z}) = \begin{cases} \mathbf{z} & \text{if } q_\phi(\mathbf{z}) \geq 0 \\ \mathbf{z} \cdot f^{-1}(f(\|\mathbf{z}\|) - f(r_{2k+1}) + k\delta/n) & \text{otherwise, for } k \text{ such that } \|\mathbf{z}\|_2 \in [r_{2k+1}, r_{2k+2}) \end{cases} \quad (40)$$

which moves the mass in  $[r_{2k+1}, r_{2k+2})$  to  $[r_{2k}, r_{2k+1})$ . From this definition, we have that  $\|\hat{T}(\mathbf{z}) - \mathbf{z}\|_2 \leq \max_{k \in \{0, \dots, n-1\}} (r_{2k+2} - r_{2k})$ . Moreover, since by definition,

$$2\delta/n = \int_{B(0, r_{2k+2})} p_\theta(\mathbf{z}) d\mathbf{z} - \int_{B(0, r_{2k})} p_\theta(\mathbf{z}) d\mathbf{z} \quad (41)$$

$$> \pi(r_{2k+2}^2 - r_{2k}^2) \min_{\mathbf{z}: \|\mathbf{z}\| \in [r_{2k}, r_{2k+2})} p_\theta(\mathbf{z}) \quad (42)$$

$$> \pi(r_{2k+2} - r_{2k})^2 \min_{\mathbf{z}: \|\mathbf{z}\| \in [r_{2k}, r_{2k+2})} p_\theta(\mathbf{z}) \quad (43)$$

We have that

$$W_2(q_\phi(\mathbf{z}), 2p_\theta(\mathbf{z})) \leq \max_{k \in \{0, \dots, n-1\}} (r_{2k+2} - r_{2k})^2 < \frac{2\delta}{\pi n \min_{\mathbf{z}: \|\mathbf{z}\|_2 \leq r_{2n}} p_\theta(\mathbf{z})} \quad (44)$$

$$< \frac{2\delta}{\pi n \min_{\mathbf{z}: \|\mathbf{z}\|_2 \leq r_{2n}} p_\theta(f^{-1}(2\delta)\mathbf{n})} \quad (45)$$

for any vector  $\mathbf{n}$  with norm 1. Note that the above inequality is inversely proportional to  $n$ , which can be any integer. Therefore, for a fixed  $\delta$ ,  $W_2(q_\phi(\mathbf{z}), 2p_\theta(\mathbf{z})) = O(1/n)$ ; so for any  $\gamma$ , there exists  $n$  such that  $W_2(q_\phi(\mathbf{z}), 2p_\theta(\mathbf{z})) < \gamma$ , completing the proof.  $\square$

Table 6: Hyperparameters across different datasets

Hyperparameter	CIFAR-10 32x32	CIFAR-100 32x32	CelebA-64 64x64	fMoW 64x64	CelebA-HQ-256 256x256	FFHQ-256 256x256
# of epochs	1000	1000	300	300	200	100
batch size per GPU	32	32	16	16	3	3
# initial channels in enc.	128	128	64	64	24	24
spatial dims of z	16*16	16*16	32*32	32*32	64*64	64*64
# channel in z	8	8	5	5	8	8
MoCo-v2 queue size	65536	65536	65536	65536	15000	15000
Diffusion feature map res.	16,8,4,2	16,8,4,2	32,16,8,4,1	32,16,8,4,1	64,32,16,8,2	64,32,16,8,2
$\lambda^{-1}$	17500	17500	17500	17500	17500	17500
learning rate	0.001	0.001	0.001	0.001	0.001	0.001
Optimizer	AdamW	AdamW	AdamW	AdamW	AdamW	AdamW
# GPUs	8	8	4	4	8	8
GPU Type	16 GB V100	16 GB V100	12 GB Titan X	12 GB Titan X	16 GB V100	16 GB V100
Total training time (h)	24	24	120	120	96	96

**Note on DDIM prior preventing the prior hole** For a noise level  $\alpha$ , we have that:

$$q^{(\alpha)}(\mathbf{z}^{(\alpha)}) = \mathbb{E}_{\mathbf{z}^{(1)} \sim q^{(1)}(\mathbf{z}^{(1)})}[\mathcal{N}(\sqrt{\alpha}\mathbf{z}^{(1)}, (1 - \alpha)\mathbf{I})] \quad (46)$$

as  $\alpha \rightarrow 0$ ,  $D_{\text{KL}}(q^{(\alpha)}(\mathbf{z}^{(\alpha)}) \parallel \mathcal{N}(0, \mathbf{I})) \rightarrow 0$ . From Pinsker’s inequality and the definition of  $(\epsilon, \delta)$ -prior hole:

$$\delta - \epsilon \leq D_{\text{TV}}(q^{(\alpha)}(\mathbf{z}^{(\alpha)}), \mathcal{N}(0, \mathbf{I})) \leq \sqrt{\frac{1}{2} D_{\text{KL}}(q^{(\alpha)}(\mathbf{z}^{(\alpha)}) \parallel \mathcal{N}(0, \mathbf{I}))}, \quad (47)$$

we should not expect to see any  $(\epsilon, \delta)$ -prior hole where the difference between  $\delta$  and  $\epsilon$  is large.

## C Experimental details

### C.1 Architecture details and hyperparameters used for training

We modify the NVAE [88] architecture by removing the “Combiner Cells” in both encoder and decoder. For the diffusion model, we use the same architecture with different number of channel multiplications, as used in [40, 81]. For Contrastive learning, we use the MoCo-v2 [15] algorithm with augmentations such as *RandomResizedCrop*, *ColorJitter*, *RandomGrayscale*, *RandomHorizontalFlip*.

Additional details about the hyperparameters used are provided in Table 6.

### C.2 Additional details for conditional generation

For  $r_\psi(\mathbf{c}|\mathbf{z}^{(1)})$  we consider training a linear model over the latent space, which has the advantage of being computationally efficient. For conditional generation on labels, we reject samples if their classifier return are lower than a certain threshold (we used 0.5 for all our experiments). For conditional image manipulation, we consider the same step size  $\eta$  for each attribute:  $\eta = 10$  for *red lipstick* and  $\eta = 15$  for *blond*. We note that these values are not necessarily the optimal ones, as the intensity of the change can grow with a choice of larger  $\eta$  values.

### C.3 Amazon Mechanical Turk procedure

The mechanical turk evaluation is done for different attributes to find out how evaluators evaluate the different approaches. The evaluators are asked to compare a pair of images, and find the best image, which retains the identity as well as contains the desired attribute. Figure 7 a) shows the instructions that was given to the evaluators before starting the test and Figure 7 b) contains the UI shown to the evaluators when doing comparison. Each evaluation task contains 10 pairwise comparisons, and we perform 15 such evaluation tasks for each attribute. The reward per task is kept as 0.25\$. Since each task takes around 2.5 mins, so the hourly wage comes to be 6\$ per hour.



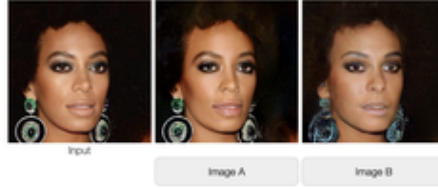
**About this HIT:**

- Please only participate in this HIT if you have normal color vision.
- It should take about 2 minutes.
- You will take part in an experiment involving visual perception. You'll see a series of 2 images. The images have been generated by 2 different Computer Programs. Given an image of a person, select out of the two images which of them best corresponds to **same person** with blond hair
- Choose the image that retains the same face, eye, earring, background as the original image, and in addition has blond hair
- You will complete a short practice (less than 1 minute) before starting the main task.

Start!

a)

Given an image of a person, select out of these two images which of them has the same face, eye, earring, background as the original image, and in addition has blond hair



b)

Figure 7: a) Instructions shown to human evaluators for Amazon Mechanical Turk for blond hair before starting the evaluation and b) UI shown to the evaluators when doing comparison.

## D Additional Results

We list results for unconditional CIFAR-10 image generation for various types of generative models in Table 7. While our results are slightly worse than state-of-the-art diffusion models, we note that our D2C models are trained with relatively fewer resources than some of the baselines; for example, our D2C models is trained on 8 GPUs for 24 hours, whereas NVAE is trained on 8 GPUs for 100 hours and DDPM is trained on v3-8 TPUs for 24 hours. We also note that these comparisons are not necessarily fair in terms of the architecture and compute used to produce the samples.

We list additional image generation results in Figure 8 (unconditional), Figures 9, 10, 11, and 12 (conditional on manipulation constraints), and Figures 13, 14, 15, and 16 (conditional on labels)<sup>10</sup>.

## E Broader Impact

Recent approaches have trained large vision and language models for conditional generation [71]. However, training such models (*e.g.*, text to image generation) would require vast amounts of resources including data, compute and energy. Our work investigate ideas towards reducing the need to provide paired data (*e.g.*, image-text pairs) and instead focus on using unsupervised data.

Since our generative model tries to faithfully reconstruct training images, there is a potential danger that the model will inherit or exacerbate the bias within the data collection process [80]. Our method also has the risk of being used in unwanted scenarios such as deep fake. Nevertheless, if we are able to monitor and control how the latent variables are used in the downstream task (which may be easier than directly over images, as the latent variables themselves have rich structure), we can better defend against unwanted use of our models by rejecting problematic latent variables before decoding.

Table 7: CIFAR-10 image generation results.

Method	FID
NVAE [88]	51.71
NCP-VAE [3]	24.08
EBM [29]	40.58
StyleGAN2 [47]	3.26
DDPM [40]	3.17
DDIM [81]	4.04
D2C	10.15

<sup>10</sup>We will list more results online after publication.



Figure 8: Additional image samples for the FFHQ-256 dataset.



Figure 9: Image manipulation results for *blond hair*.



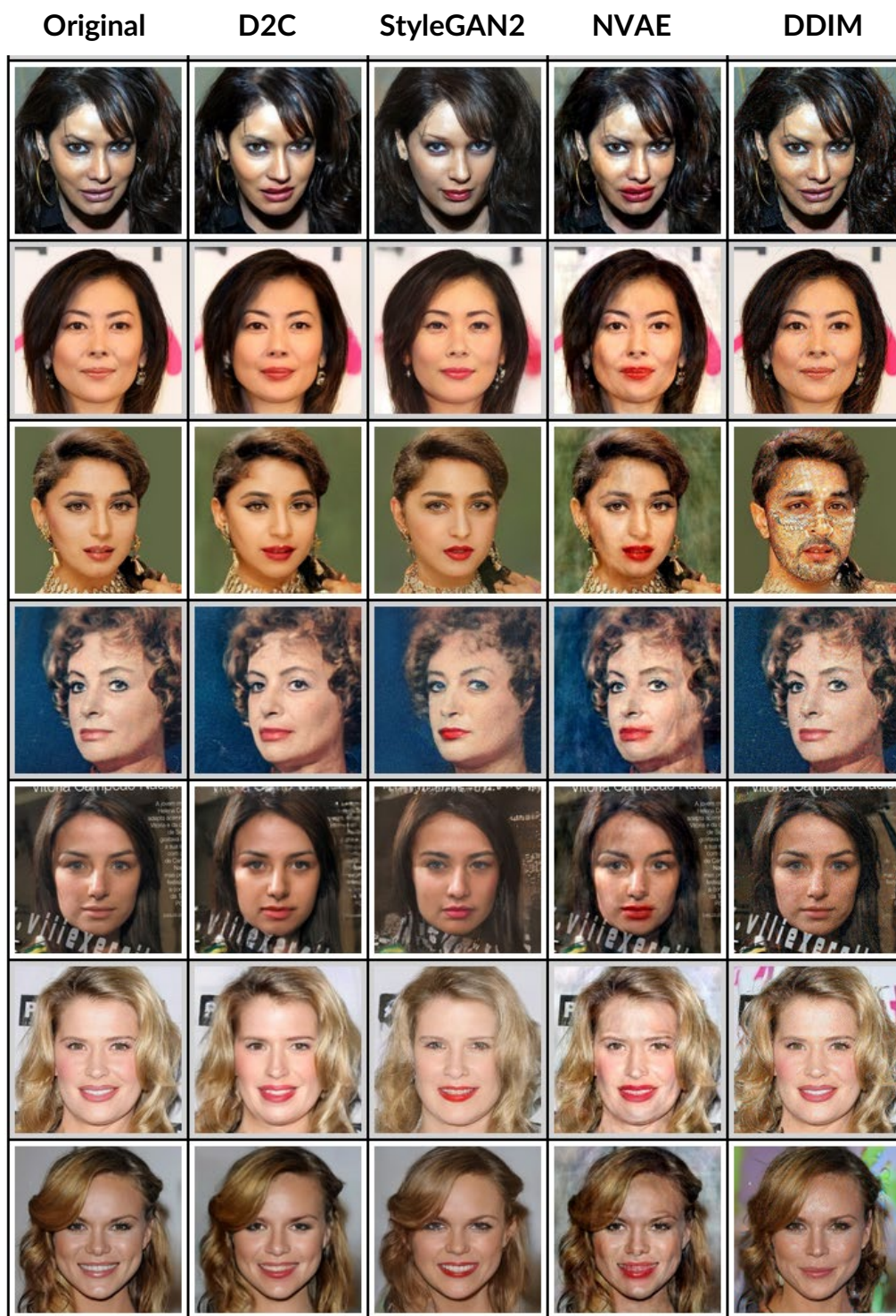


Figure 10: Image manipulation results for *red lipstick*.

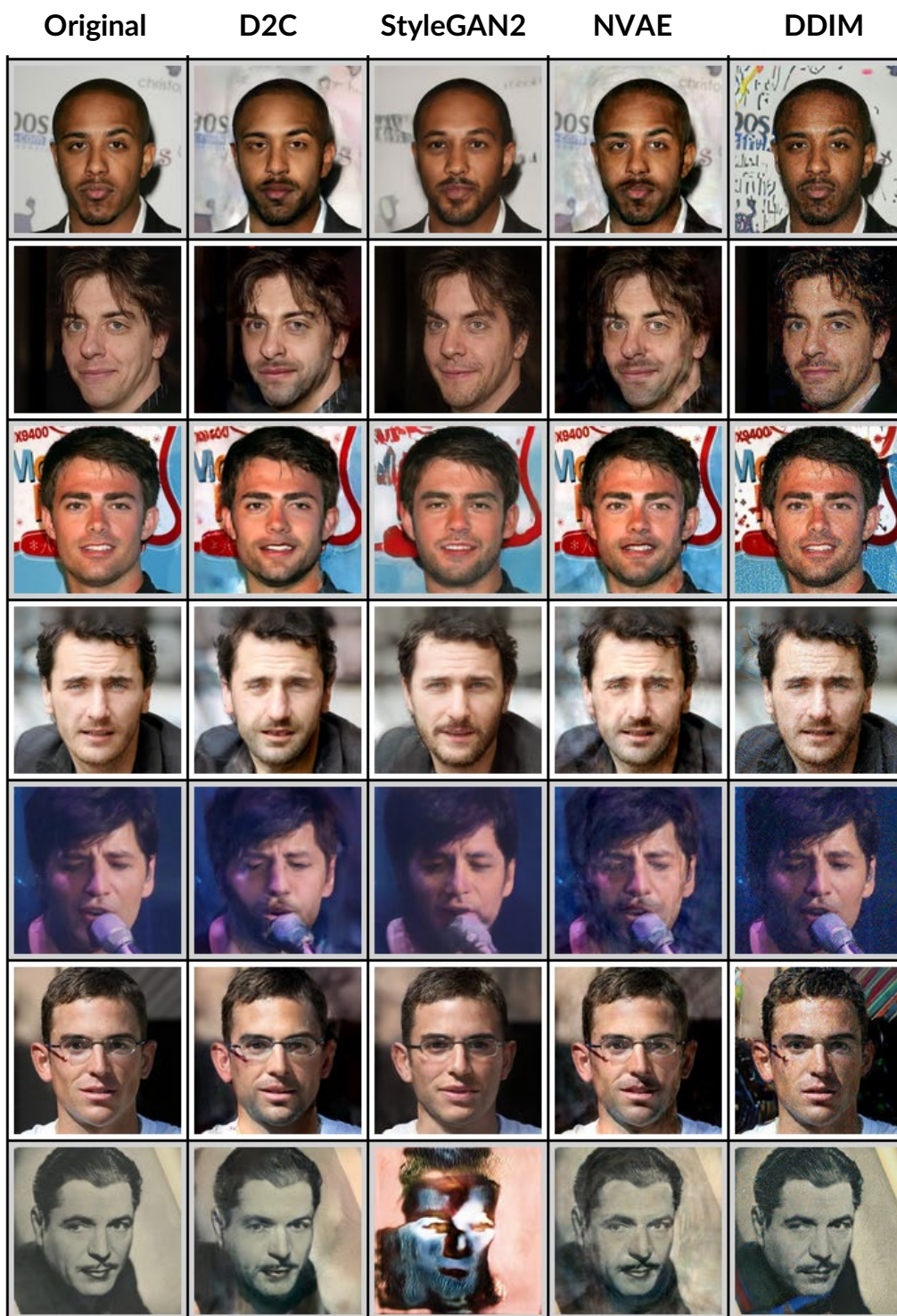


Figure 11: Image manipulation results for *beard*.



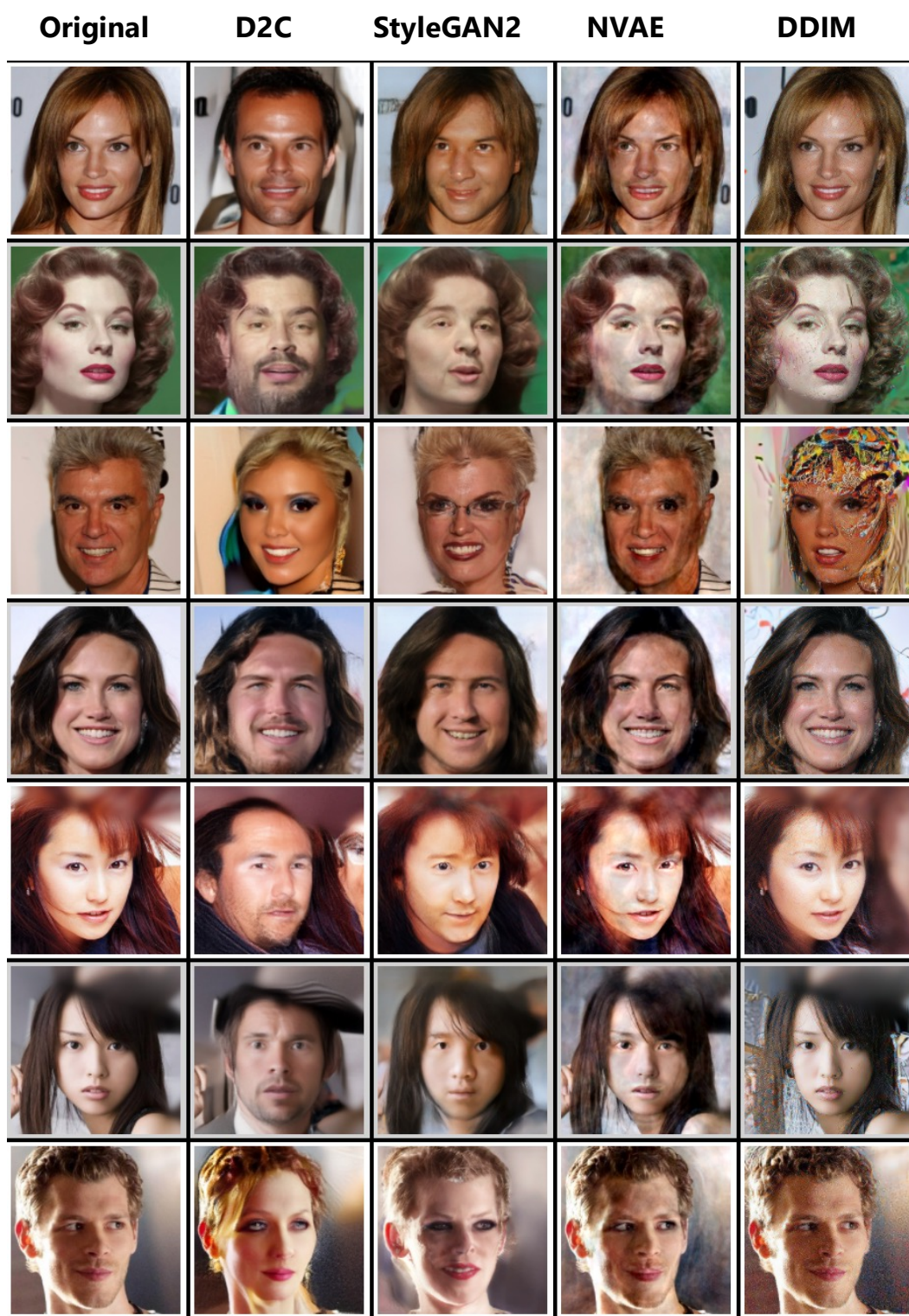


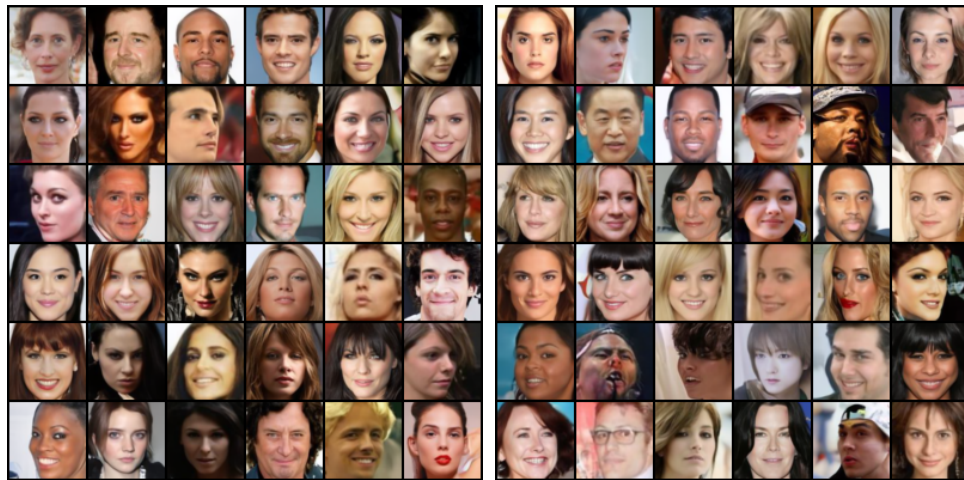
Figure 12: Image manipulation results for *gender*.



(a) Conditioned on *non-blond* label

(b) Conditioned on *blond* label

Figure 13: Conditional generation with D2C by learning from 100 labeled examples.



(a) Conditioned on *non-blond* label

(b) Conditioned on *blond* label

Figure 14: Conditional generation with DDIM by learning from 100 labeled examples.





(a) Conditioned on *female* label

(b) Conditioned on *male* label

Figure 15: Conditional generation with D2C by learning from 100 labeled examples.



(a) Conditioned on *female* label

(b) Conditioned on *male* label

Figure 16: Conditional generation with DDIM by learning from 100 labeled examples.